Title

Precisely timed theta oscillations are selectively required during the encoding phase of memory

Journal

Nature Neuroscience, 24(11)

ISSN

1097-6256

Authors

Quirk, Clare R
Zutshi, Ipshita
Srikanth, Sunandha
et al.

Publication Date

2021-11-01

DOI

10.1038/s41593-021-00919-0

Peer reviewed

HHS Public Access

Author manuscript

Nat Neurosci. Author manuscript; available in PMC 2022 April 04.

Published in final edited form as:

Nat Neurosci. 2021 November ; 24(11): 1614–1627. doi:10.1038/s41593-021-00919-0.

Precisely Timed Theta Oscillations are Selectively Required During the Encoding Phase of Memory

Clare R. Quirk[1,†], **Ipshita Zutshi**[1,†], **Sunandha Srikanth**[1], **Maylin L. Fu**[1], **Naomie Devico Marciano**[1], **Morgan K. Wright**[1], **Darian F. Parsey**[1], **Stanley Liu**[1], **Rachel E. Siretskiy**[1], **Tiffany L. Huynh**[1], **Jill K. Leutgeb**[1], **Stefan Leutgeb**[1,2,*]

[1]Neurobiology Section and Center for Neural Circuits and Behavior, University of California, San Diego, La Jolla, CA 92093, USA

[2]Kavli Institute for Brain and Mind, University of California, San Diego, La Jolla, CA 92093, USA

Abstract

Brain oscillations have been hypothesized to support cognitive function by coordinating spike timing within and across brain regions, yet it is often not known when timing is either critical for neural computations or an epiphenomenon. The entorhinal cortex and hippocampus are necessary for learning and memory and exhibit prominent theta oscillations (6–9 Hz), which are controlled by pacemaker cells in the medial septal area (MSA). Here we show that entorhinal and hippocampal neuronal activity patterns were strongly entrained by rhythmic optical stimulation of parvalbumin-positive MSA neurons in mice. Despite strong entrainment, memory impairments in a spatial working memory task were not observed with pacing frequencies at or below the endogenous theta frequency and only emerged at frequencies ≥10 Hz and specifically when pacing was targeted to maze segments where encoding occurs. Neural computations during the encoding phase were therefore selectively disrupted by perturbations of the timing of neuronal firing patterns.

Oscillatory neuronal activity and rhythmic neuronal spiking are prominent features of information processing in neural circuits that are thought to be critical for cognitive processing[1–3]. Despite a vast literature on correlations between oscillatory patterns and cognitive function, it has been challenging to establish causality because manipulations that are aimed at disrupting oscillations often also have effects on non-oscillatory patterns, including neuronal firing rates and sparsity. These effects may be undetermined when

*Correspondence should be addressed to S.L. (sleutgeb@ucsd.edu).
†These authors contributed equally to this work

AUTHOR CONTRIBUTIONS

C.R.Q., I.Z., J.K.L., and S.Leutgeb conceived experiments, designed study, and interpreted data. C.R.Q., M.K.W., D.F.P., M.L.F., S.Liu, N.D.M., R.E.S., and T.L.H. collected data from the spatial alternation task and performed recordings in the open field. I.Z., C.R.Q., M.L.F., R.E.S., and T.L.H. performed recordings on the rectangular track. I.Z., C.R.Q., and S.Leutgeb analyzed single cell recording data, S.S. and S.Leutgeb analyzed LFP recording data, and C.R.Q. and S.Leutgeb analyzed behavior data. C.R.Q., I.Z., J.K.L., and S.Leutgeb prepared figures and wrote the manuscript. J.K.L., and S.Leutgeb managed the project.

COMPETING INTERESTS STATEMENT

The authors declare no competing interests.

neuronal activity levels are not measured or even be intended when the method for disrupting oscillations is transient silencing[4–6]. It is thus challenging to selectively alter the timing of network oscillations along with examining whether other aspects of the neuronal code remain intact. In contrast to many other oscillation patterns in the brain, theta oscillations are governed by pacemaker cells in an anatomically well-separated brain region[7–9], which provides an exceptional opportunity to selectively manipulate the timing of neural circuits. These pacemaker cells are located in the medial septal area (MSA) and consist of rhythmically bursting GABAergic cells that prominently project to inhibitory interneurons in the hippocampus[10–12]. A subset of these septal GABAergic cells are PV positive neurons[13–16], and the rhythmic activation of PV cells is sufficient to generate rhythmic potentials in the hippocampus[17, 18] that supersede endogenous theta oscillations[19].

However, an understanding of the role of septal projections for pacing hippocampal oscillations is not complete without determining the function of septal projections to the medial entorhinal cortex (mEC). The projections of MSA GABA cells to mEC and hippocampus share the feature that they predominantly terminate on local inhibitory interneurons in both regions[10–12, 20, 21]. Furthermore, septal lesions or inactivations disrupt theta oscillations not only in hippocampus, but also in mEC[22–26]. Importantly, MSA projections do not only directly generate theta in mEC, but mEC theta is in turn critical for hippocampal theta generation[22, 27–2925, 26]. In order to comprehensively understand how manipulations of local field potential (LFP) oscillations alter neuronal activity patterns in the entorhino-hippocampal circuit, it is thus necessary to identify the effects of septal manipulations on not only hippocampal, but also on mEC temporal and spatial firing patterns. We therefore performed LFP and single unit recordings in freely behaving mice while rhythmically stimulating MSA PV neurons and examined how paced theta-like oscillations alter the spike timing and the spatial firing patterns of mEC cells, and for comparison, of hippocampal cells. Based on previous findings that disrupting theta oscillations by medial septal lesion or inactivation disrupt memory[8, 30], we then used septal pacing to test theories that have proposed that theta oscillations are critical for memory encoding, retention, and retrieval[31–33]. Entrainment of theta oscillation to the optical septal stimulation occurred with stimulation frequencies from 4 Hz to 20 Hz, but memory performance was only impaired when the oscillatory frequency within the mEC-hippocampus circuit was shifted to frequencies ≥ 10 Hz, which is higher than the endogenous theta range. Importantly, theta frequency was not critical during all behavioral phases in which theta-related neuronal activity is prominent[32–34], but manipulations of theta frequency had a task-phase selective effect.

RESULTS

Optogenetic stimulation of MSA PV cells controls theta frequency

Rhythmic stimulation of septal projections to the hippocampus is known to control hippocampal LFP oscillations[17–19]. In addition, septal projections also terminate in mEC[20, 21], and we therefore predicted that a manipulation which controls hippocampal oscillations[19] also controls mEC theta oscillations. To compare the effects of optogenetic pacing of MSA PV neurons on LFP between hippocampus and mEC, we expressed ChR2

in the MSA of PV-cre mice and confirmed that ChR2 expression was restricted to the MSA (Fig. 1a and b). Electrophysiological recordings from mEC and hippocampus were performed in mice running on a rectangular track and/or in an open field (Fig. 1c). Rhythmic optical stimulation at 8, 10, or 12 Hz was delivered to the MSA on every other lap on the track or, in the open field, for ~10-min long sessions between two sessions without stimulation so that neuronal activity could be compared between periods with and without stimulation. The hippocampal LFP recordings replicated our previously published observations[19] that optogenetic activation of MSA PV cells effectively controls hippocampal oscillations and replaces endogenously generated theta oscillations (Fig. 1d and Extended Data Fig. 1a; median peak LFP frequency with 8, 10 and 12 Hz stimulation: 7.9, 9.9, and 12.0 Hz). Similar to the effects in hippocampus, rhythmic stimulation of MSA PV cells directly controlled the frequency of mEC oscillations and superseded endogenous theta (Fig. 1d and e and Extended Data Fig. 1a; median peak LFP frequency with 8, 10 and 12 Hz stimulation: 8.0, 10.1, and 11.8 Hz). Running speed was not altered by MSA stimulation either in the open field or on the rectangular track (Extended Data Fig. 2).

Based on the finding that mEC and hippocampal oscillations are similarly paced by MSA stimulation, we next sought to determine whether hippocampal theta-like oscillations during MSA stimulation remain predominantly generated by a combination of direct inputs from MSA to hippocampus and indirect inputs via the entorhinal cortex, or whether artificial pacing by synchronously activating septal PV neurons shifted patterns of theta oscillations across hippocampal layers[16]. We implanted linear silicon probes into the hippocampus, recorded the LFP at 16 sites spaced 50 μm apart, and performed current source density analysis. The main sink/source pair during paced oscillations remained in the stratum lacunosum-moleculare (slm), where excitatory inputs from the mEC to the hippocampus terminate (Extended Data Fig. 3). These results confirm that the main generator for hippocampal theta-like oscillations likely remains a combination of excitatory inputs from entorhinal cortex and direct input from MSA without a major shift in the balance of these sources[27, 28].

Firing patterns of mEC cells became strongly entrained

Given that mEC cells project to the hippocampal slm layer[35] and that current sinks are thought to be generated by synchronous synaptic activity[36], we reasoned that mEC excitatory cells should oscillate at frequencies that closely correspond to the LFP frequency that was recorded in the hippocampus. To determine the oscillatory firing patterns of excitatory mEC cells (see Extended Data Fig. 1b for criteria), we analyzed mEC cells that were recorded as mice ran in an open field arena or on a rectangular track. We first measured to what extent the amplitude of the oscillatory modulation of mEC cell spiking was altered by septal stimulation by generating a temporal autocorrelation of the spike train and performing a fast-Fourier transform (FFT) for stimulation and no-stimulation periods (Fig. 2a). There was an increase in the amplitude of the oscillatory modulation of spike trains in periods with stimulation compared to periods without stimulation in the mEC (Fig. 2b). While hippocampal cells may also become coupled to paced LFP oscillations, we previously showed that the majority of hippocampal cells are not directly entrained by paced oscillations[19]. To confirm these results, we performed additional hippocampal

recordings. In contrast to mEC, the amplitude of oscillatory modulation of the spike trains of hippocampal principal cells did not change at any of the stimulation frequencies for hippocampal principal cells (Fig. 2c and d).

Principal cells in mEC responded directly to MSA pacing

Given that the spiking of mEC cells became entrained at high amplitude to optically paced oscillation frequencies, we expected that the predominant spiking frequency of mEC cells would be tightly locked to the stimulation frequency. Because frequency cannot be accurately estimated at very low oscillation amplitudes, we remove cells with little to no oscillatory modulation (power <0.1, <20 % of mEC cells). Using the peak frequency of the remaining cells, we found that mEC principal neurons shifted their entrainment towards frequencies that closely matched the stimulation frequency (Fig. 3a and b). The entrainment of spiking to the stimulation frequency occurred irrespective of the cell's oscillation frequency at baseline (Fig. 3b, bottom). Similar to mEC cells, oscillation frequencies of spike trains of hippocampal principal cells were also strongly modified by pacing, but with hippocampal cells retaining a difference from the stimulation frequency, which was larger than in mEC (Fig. 3c and d). Consistent with the closer match between spike train oscillation frequency and stimulation frequency in the mEC compared to the hippocampus, we also found that the relative increase in firing rate following the onset of the optical stimulation was higher in mEC principal cells than in hippocampal CA1 principal neurons (Fig. 4a and b). Furthermore, phase locking of spiking to LFP more readily increased during stimulation compared to baseline in mEC at 8 Hz and 10 Hz, but not at 12 Hz (Fig. 4c). The opposite pattern was found in hippocampus, where there was no change at 8 Hz or 10 Hz, but an increase at 12 Hz (Fig. 4d). This pattern is consistent with an increasingly more synchronizing effect of pacing on hippocampal cells at higher stimulation frequencies.

Hippocampal and mEC interneurons responded directly to MSA pacing

Because medial septal GABAergic neurons are known to directly project to interneurons rather than principal cells in mEC and hippocampus[10, 21] and to elicit disinhibition of excitatory cells by inhibiting inhibitory interneurons, we reasoned that we might identify at least a subclass of interneurons in mEC and hippocampus that are strongly coupled to septal stimulation. The majority of mEC and hippocampal interneurons shifted their spike trains' oscillation frequencies during pacing such that the frequency during pacing was approximately matched to the stimulation frequency. As a consequence, interneurons in mEC and hippocampus were similarly entrained. Moreover, interneurons generally showed high amplitude theta modulation at baseline, and a further increase compared to baseline was only observed at a subset of stimulation frequencies (Extended Data Fig. 4).

Effects on spatial firing were matching across pacing frequencies

Given the substantial effects on the timing of LFP oscillations and the strong coupling of mEC cells to the optical stimulation, we examined the effects of MSA stimulation on spatial coding of mEC principal cells. We had previously observed in GFP control mice that the spatial firing patterns of hippocampal place cells remapped on a rectangular track between alternating laps with light-stimulation on and light-stimulation off[19], and now found that spatially modulated mEC cells also remapped in GFP control mice (Extended

Data Fig. 5a–d). To test whether additional effects would be obtained when oscillations were paced at 8 Hz and 12 Hz, we performed mEC recordings (Fig. 5a–f) and a new set of hippocampal recordings (Fig. 5g–l) on the rectangular track in mice with ChR2 expression in MSA. For both 8 and 12 Hz pacing, spatial correlations across laps differed between four types of comparisons (within light-off, within light-on, between light-off/on, with cell identify shuffled; mEC, Fig. 5b; hippocampus, Fig. 5h), which indicates that remapping remained partial (i.e., between light-off/on value is higher than for shuffle but lower than within light-off and within light-on values). In addition, high values for within light-off stability and within light-on stability indicate stable spatial organization within each condition. There were also other effects on spatial firing properties, but these were similar between stimulation frequencies. The number of fields per cell decreased with 8 and 12 Hz stimulation (mEC, Fig. 5d; hippocampus, Fig. 5j). There was a significant increase in spatial information in mEC with both 8 Hz and 12 Hz pacing (Fig. 5c), while there was no change in spatial information in the hippocampus at either stimulation frequency (Fig. 5i). In mEC, there was no change in mean or peak firing rate between laps with and without pacing (Fig. 5e), while in the hippocampus, there was a decrease in both mean and peak firing rate with pacing at 8 Hz and at 12 Hz (Fig. 5k). The same pattern of effects on spatial firing properties as with nonparametric statistics (Fig. 5) was also seen when using two-way ANOVAs with light stimulation (on vs off) and stimulation frequency (8 Hz vs 12 Hz) as factors (Supplementary Table 1). While there were effects of light simulation, as described above, there we no effects of stimulation frequency or any interactions. The effects of optical pacing on spatial firing in mEC and hippocampus were thus matching between the 8 Hz and 12 Hz stimulation frequencies and were also largely corresponding to effects with light delivery in GFP control mice (ref. 19 and Extended Data Fig. 5a–d).

We also tested whether remapping occurred in an open field for spatially modulated mEC cells. In the open field, each recording sequence consisted of 3–5 recording sessions, which each lasted 10–15 minutes. The sequence began and ended with baseline sessions without optical stimulation. Optical stimulation at either 8 Hz, 10 Hz, or 12 Hz was applied during the intervening sessions (Fig. 6a) and resulted in a minor decrease of firing rates of principal cells and interneurons (Fig. 6b, Extended Data Fig. 6). For spatially modulated cells, light stimulation resulted in remapping (Fig. 6c) and in reduced within-session stability of irregular spatial cells during stimulation compared to baseline sessions (Fig. 6d). In addition, there was a decrease in spatial information during light stimulation sessions (Fig. 6d), which differed from the minor increase on the rectangular track (see Fig. 5). These effects on spatial firing properties were not detected with light stimulation in control mice with GFP expression in the medial septal area (Extended Data Fig. 5f and g and Supplementary Table 2), which suggests that pacing of oscillations at the tested frequencies alters entorhinal spatial firing patterns in the open field, but to a similar extent across stimulation frequencies.

Grid, head-direction, and speed cells remained unaffected

Because the recordings in the open field afforded us to detect effects of paced oscillations on specialized mEC firing patterns, we separated mEC principal cells by cell type (i.e., grid cells, head-direction cells, speed cells) and compared baseline to stimulation sessions. Cells were assigned to a functional cell type when their firing modulation exceeded the 95th

percentile of shuffled values in any two recording sessions with or without light stimulation. The inclusion of all recording sessions for determining cell type avoided a bias that would be introduced by applying the criterion to only baseline sessions, but can result in cells' values below criterion in some pre-stimulation or post-stimulation baseline sessions. For grid cells, there was no change to the spatial information (Fig. 6e), spatial periodicity (Fig. 6e), or the spacing of grid fields (Fig. 6g) by the pacing of oscillations. Neither did the grid alignment shift during pacing compared to the no-stimulation baseline (Fig. 6f). Similarly, neither sharply nor broadly tuned head direction (HD) cells altered the magnitude of their directional tuning during pacing at any stimulation frequency (Fig. 7a and b). Furthermore, the preferred direction did not shift during pacing compared to the no stimulation baseline (Fig. 7c and d). Speed coding has been described for principal cells and interneurons[37] and was not disrupted for either class of cells at any of the stimulation frequencies (Fig. 7e and f).

Paced frequencies ≥ 10 Hz resulted in memory impairment

Given that pacing of theta-like oscillations did not result in disruptions of grid, head-direction, and speed cells in mEC and resulted in matching disruptions of spatial firing across pacing frequencies, while yielding substantial shifts in LFP frequency in mEC and hippocampus and entrainment of mEC cells to the stimulation frequency, we proceeded to analyze whether manipulations that substantially altered the timing of mEC firing patterns impaired memory. The spatial alternation task is known to depend on hippocampus and mEC when a delay is introduced, but not when running is continuous[38, 39]. We therefore used the continuous version of the task as a control while also training mice on delayed versions (2 s delay and 10 s delay). To receive a food reward, mice had to alternate between left and right choices in a figure-8 shaped maze, and during each day, blocks of 10 trials without stimulation were interleaved with blocks of 10 trials with stimulation (Fig. 8a and b). One of six stimulation frequencies (4, 6, 8, 10, 12, or 20 Hz) was used on each test day, and each mouse was tested for 2–3 days at 3–4 of the stimulation frequencies (in pseudorandom order across days). Pacing efficiency was consistently high in all mice, but we further ensured that pacing was efficient by excluding behavioral sessions at any stimulation frequency at which the pacing efficiency score was below 0.2 (Extended Data Figs. 7 and 8). In addition, pacing did not result in systematic effects on running speed in any maze segment (delay, stem, reward zone, return arms; Extended Data Fig. 2).

During behavioral testing in the spatial alternation task, mice performed significantly above chance at any of the delay conditions without stimulation (two-sided Wilcoxon signed rank test against chance level of 50 %, ChR2/oChIEF group: $n = 28$, all P values < 0.001). We next compared behavioral performance between blocks with and without stimulation. There were no significant differences for any of the stimulation frequencies in the no delay condition (Fig. 8c, Extended Data Fig. 9, and Supplementary Table 3), consistent with previous evidence that the hippocampus as well as the mEC are not necessary for performance of the task without delay[38, 39]. While there was no impairment in the task version without delay, we found that stimulating at 10, 12, and 20 Hz significantly impaired memory performance in the versions with a 2 s delay and a 10 s delay (Fig. 8c). However, we did not detect a correlation between pacing efficiency and the decrease in memory

performance at any of these stimulation frequencies (Extended Data Fig. 9). Stimulating at 8 Hz did not result in a memory impairment during either delay condition (2 s and 10 s delay), even though 8 Hz stimulation had comparable effects on spatial firing patterns as higher stimulation frequencies. In addition, we did not detect a memory impairment with stimulation frequencies of 4 Hz and 6 Hz (Extended Data Fig. 8).

We next controlled for any behavioral perturbation that could have been caused by the light stimulation alone. Nine animals injected with ChR2 were tested while stimulation with green light (532 nm) was delivered. This wavelength is known to weakly activate ChR2[40], and to be confident to only include animals without evidence of pacing in the control analysis, we excluded all animals with pacing scores >0.1 (n = 5 of 9). The remaining control animals were mice that expressed a cre-dependent GFP vector (AAV.EF1a.DIO.eGFP) and received blue light stimulation (473 nm). In all control animals combined (n = 4 ChR2 mice with green light delivery; n = 10 with GFP expression), there were no significant differences in performance between blocks with and without stimulation (Fig. 8c). The same results were also obtained when separately analyzing only the animals with GFP expression (Supplementary Table 3). These controls demonstrate that behavioral impairments were due to disruption by the pacing of endogenously paced theta oscillations and not due to disruption of behavior by other possible effects of light delivery.

Selective spatial memory impairment by pacing on return arms

Theta oscillations have long been hypothesized to have roles in memory encoding as well as retrieval[31, 32]. In order to test whether altered theta oscillation frequency was critical during different periods of the memory task, we limited light stimulation to segments of the maze, which were chosen by their presumptive role in either encoding or retrieval. In the spatial alternation task, a successful subsequent choice depends on the correct encoding of the previous trajectory. In particular, information about the trajectory can be encoded while the animal is returning to the delay zone on either the left or right maze arms. After the delay zone on the center arm has been reached, information about the path is no longer directly available from sensory information but rather has to be retained and/or retrieved from memory. We therefore performed stimulation on arm segments in which left/right information is available (i.e., return arms) as opposed to segments in which information needs to be retained (stem segment including delay). As additional controls, we also stimulated in the zone where reward is delivered including arm segments after the T junction or on all segments beginning before the delay and ending after reward consumption (Fig. 8d). We confirmed that we were able to reliably shift LFP oscillations to the stimulation frequency of 12 Hz in the targeted zone and that the amplitude of the evoked oscillations did not differ across maze zones (Extended Data Fig. 10). We found that a frequency shift only impaired working memory performance when applied to the return arm segments during trials with a 10 s delay (Fig. 8e). A trend towards impairment was observed with a 2-s delay and no effect was found without delay. There were no effects of optical stimulation when delivered to any of the other targeted maze segments (reward, delay+stem, delay+stem+reward) for any of the delay conditions. Notably, the selective effect of stimulation in the return arms occurred even though the time spent in this phase of the behavior was comparable to the reward and delay+stem and shorter than in the

delay+stem+reward zone in the 10 s delay condition (Extended Data Fig. 10). These results suggest that paced theta oscillations at frequencies higher than the endogenous theta range have a preferential role in disrupting memory when targeted to arm segments in which task-relevant information can be encoded. Interestingly, there was no effect on performance when optical stimulation was delivered in any other zone of the maze, including the delay zone and stem, where animals had to retain/retrieve memory about the previous path to make a subsequent correct choice.

DISCUSSION

Cognitive function is thought to require the temporally precise coordination of neuronal activity[1–3]. The control of theta oscillations by pacemaker cells in the MSA[7–9, 12] provides for an opportunity to selectively manipulate oscillatory patterns. Here we show that rhythmic optogenetic stimulation of MSA PV cells controlled theta-like oscillations in mEC, and we replicated previous reports that septal stimulation controls the frequency of hippocampal LFP oscillations[17–19, 41]. By also recording cells in mEC as well as the depth profile of the hippocampal LFP, we found that mEC cells were strongly entrained by septal PV cells and that the most prominent current source remained in the termination zone of the entorhinal projections to hippocampus. The entrainment of mEC cells to the pacing frequency thus appears to contribute to the generation of paced LFP oscillations to a corresponding extent as during endogenous theta oscillations. Despite the major control over entorhinal and hippocampal firing patterns by septal stimulation, which resulted in substantial differences in the temporal organization between stimulation frequencies, effects on firing rates and the precision of spatial firing patterns typically corresponded between 8 Hz stimulation and 12 Hz stimulation frequencies and to those observed with control light stimulation[19]. Given that the reorganization of predominantly temporal rather spatial firing patterns differed across stimulation frequencies, we examined the behavioral consequences of paced oscillations across a range of frequencies using an mEC-dependent and hippocampus-dependent spatial working memory task[38, 39]. We found that the increased synchrony and any effects on spatial firing that were generated in mEC by septal stimulation was not sufficient to disrupt memory when the stimulation frequency was within or below the endogenous theta range. Memory impairment only began to emerge when the evoked frequency was higher than the endogenous theta range and was particularly pronounced with 12 Hz or 20 Hz stimulation. Furthermore, the oscillation frequency of the mEC-hippocampal circuit was only critical during task phases during which task-relevant information could be encoded. The selective effect for only manipulations on the return arm indicates that a substantial reorganization of spike timing, such as an increase in amplitude of mEC principal cells and a shift in the intrinsic frequency of both mEC and hippocampal principal cells during other task phases, does not preclude successful memory performance.

While we thus found that our manipulations of theta oscillations effectively impaired spatial memory during one of the task phases when endogenous theta oscillations are prominent, we did not find an effect during other task phases in which endogenous theta oscillations are equally pronounced and have been hypothesized to contribute to working memory retention and to decision making[32, 33]. In particular, we found that profound perturbations of oscillatory patterns were without behavioral consequences when limited to behavioral

phases during which memory needed to be retained and a choice needed to be selected. While our data thus support a long-hypothesized role for theta oscillation frequency in memory encoding, they also show that later phases of memory processing are highly tolerant to major shifts in the oscillatory frequency. However, oscillatory activity is not only tied to precisely timed sequences of neuronal activity but also thought to support synchrony by narrowing the time window during which cells are active. Importantly, increased memory-related synchrony has been reported in the theta and gamma ranges during the retrieval phase of spatial memory tasks[32, 42]. Furthermore, contextual memory can be reinstated by optogenetic manipulations that certainly do not resemble any of the circuit's timed neuronal activity, but rather yield synchronous activation of hippocampal cell populations[43]. While our manipulation effectively shifts oscillation frequencies, it also causes neuronal firing patterns, in particular in mEC, to become more synchronous at any stimulation frequency. The lack of effectiveness of septal pacing on behavior during the retention/retrieval phase of working memory therefore suggests that the precise frequency of theta oscillations is not critical, but does not exclude the possibility that the increased temporal synchrony that oscillations provide within and across brain regions may be required during task phases in which memory is retained or retrieved.

Furthermore, the possibility also needs to be considered that encoding of the previous arm choice already begins in the reward zone of the previous trial and that the retention of memory for the previous choice is then disrupted in conditions with accelerated theta frequency on the return arms. In this scenario, it would not be an encoding mechanism that is impaired by the altered oscillations but rather the retention while returning to the delay zone. While this is a possible interpretation, it would imply that mechanisms of retention differ between zones on the maze, because we found that the same manipulation was not effective in disrupting retention when applied in the delay zone and on the stem. Similar reasoning also applies to a scenario that assumes that the information is not continuously retained but rather encoded and subsequently retrieved. If the encoding were to take place in the reward zone and the key mechanism on the return arms is the retrieval of information, it would need to be assumed that subsequent retrieval cannot occur in the delay zone and on the stem for memory to be impaired with only return arm stimulation. On balance, it would thus need to be assumed that either retention/retrieval mechanisms differ across different maze zones or that there is at least a partial contribution from impaired encoding of information when oscillations are selectively paced in the return arms, which is the zone when the animal's current location can inform the next choice. Consistent with the interpretation that manipulations in zones when spatial information is encoded result in a selective impairment, hippocampal projections that convey spatial information to the prefrontal cortex have been shown to be critical during encoding/sampling phases in spatial memory tasks[44].

The mEC has long been hypothesized to have at least a partial role in generating theta rhythmicity in the hippocampus. It has previously been shown that theta activity in the hippocampus is generated by both feed-forward inhibition from MSA GABAergic neurons and feed-forward excitation from the entorhinal cortex[22, 27]. Furthermore, bilateral lesions to the entorhinal cortex diminish the sink-source pair in the distal dendrites in CA1[28] and lesions of the perforant path reduce theta amplitude in the hippocampus[29]. These previous

lesion studies, along with our finding that mEC principal cells are faithfully entrained to the stimulation suggest that the entrainment of mEC cells by septal PV cells continues to make a similar contribution to paced hippocampal oscillations as to endogenous theta oscillations. These findings do not exclude the possibility that direct projections of septal PV cells to hippocampal interneurons also control hippocampal firing patterns, but it could be the case that the predominant targeting of hippocampal axo-axonic cells, which in turn target the axon initial segment, results in a lesser effect on LFP compared to action potential generation[10, 16, 45]. Furthermore, there is also a substantial population of PV-negative GABAergic cells, which project to the hippocampus and were not targeted in our experiments, but may have effects on local hippocampal activity patterns[46]. Overall, the tight coupling of mEC cells to the septal oscillation frequency is consistent with a prominent role of mEC in generating hippocampal LFP oscillations[22, 27, 28], while the oscillation frequency of the spike trains of hippocampal principal cells can simultaneously diverge[19]. These results indicate that high variability in hippocampal phase coding, such as phase precession, can persist even in conditions when the oscillations of most entorhinal cells are tightly locked to the LFP frequency.

Previous research has shown that inactivation of the MSA and subsequent reduction of theta amplitude has a selective effect on reducing the spatial firing of grid cells while other hippocampal and mEC cell types remain intact[25, 26]. Interestingly, our results and a recently published study[47] do not show any substantial alterations to grid or head-direction coding in mEC when manipulating the timing of septal oscillations. In contrast to the lack of effects with septal pacing, previous studies with pharmacological inactivation of the MSA caused a large reduction of not only theta oscillations, but also of firing rates of principal cells in the entorhino-hippocampal circuit[25, 26, 48]. The more selective manipulation of entorhinal spike timing by stimulation of septal PV cells suggests that effects on grid cells by MSA manipulations in the earlier studies may have arisen from a decrease in excitatory drive[49] and that any effects on spatial coding in mEC are much more minor when oscillation patterns are more selectively controlled.

It has generally been assumed that brain oscillation patterns in multiple frequency bands are necessary for cognitive processes and for spatial memory coding[1–3, 32, 42]. Furthermore, it has been shown in pharmacological studies and in epilepsy models that altered hippocampal spike timing rather than reorganization of spatial firing patterns is observed along with spatial memory deficits[50–54]. Here we show that brain circuits can tolerate a wide range of perturbations of oscillatory frequency and that even extensive frequency shifts that disorganized the relative timing between mEC and hippocampus did not yield memory impairments in task phases other than the return arms. We obtained these results in a task in which theta oscillations during many task phases are pronounced. Yet, oscillations on the stem, including during the choice phase, could be shifted well beyond the endogenous range without yielding any behavioral impairment. In addition, although not directly measured here, synchronous activation of septal PV neurons may also diminish travelling waves along the dorso-ventral axis of hippocampus and mEC[55, 56]. Such increased phase coupling along the axis can be assumed to not disrupt behavior when elicited to a similar extent at pacing frequencies that either show or do not show effects on behavior. While altered oscillation frequency and amplitude can undoubtedly be a sign of memory-related circuit computations

during particular task phases or of circuit dysfunction in disease models[32, 42, 57], findings that are based on LFP oscillations do not yield information on the nature of the underlying neural computations and on the necessity of the oscillatory patterns. Rather, our results show resilience of circuits to substantially altered oscillation patterns and that the identification of a link between timing-dependent neural computations and cognitive function requires rigorous testing by perturbation of the temporal organization of neural circuits.

METHODS

Subjects

Fifty-four parvalbumin-cre [129p2-Pvalbtm1(cre)arbr/j, Jackson Labs] adult mice (n = 33 male, n = 21 female; 4–12 months of age) weighing between 25–35 grams were used as subjects. The mice were housed at a temperature of 68–72 ºF and at a relative humidity of 30–70 %. Of the 54 mice, 6 were used for testing in the spatial alternation task and for mEC recordings in the open field, 33 for only testing in the spatial alternation task, and 15 for only recordings experiments in the open field and on the rectangular track (11 in mEC, 4 in hippocampus). Mice that were tested in the spatial alternation task and that were used for mEC recordings were housed on an inverse 12 hr light-dark cycle (lights off at 8 am), while mice for hippocampal recordings on the rectangular track were housed on a regular 12 hr light-dark cycle (lights on at 7 am). The hippocampal recordings were therefore conducted in the light phase, and all other experiments were conducted in the dark phase. Mice were restricted to 85% of their *ad libitum* weight and given full access to water. All procedures were conducted in accordance with the University of California, San Diego Institutional Animal Care and Use Committee.

Surgery

Mice were first injected with one of four viral vectors. Thirty-four mice with a vector expressing ChR2 (AAV.EF1α.DIO.ChR2.eGFP), 4 mice with a vector expressing oChIEF (AAV.EF1α.FLEX.oChIEF.mCitrine), and 16 mice with a vector expressing only a green fluorescent protein (AAV.EF1α.DIO.eGFP or AAV.EF1α.DIO.mEmerald). One of the mice with oCHIEF expression did not show evidence for paced LFP oscillations in response to light stimulation (average pacing score: 0.04) and was excluded from all analyses of behavioral and recording data. The other three oCHIEF mice showed pacing within the range of ChR2 mice (average pacing scores: 0.16, 0.27, 0.37) and were grouped with ChR2 mice for all analyses (except in Supplementary Table 3, which shows analysis of behavioral data in only mice with ChR2 expression). Viral vectors were provided by Dr. Byungkook Lim's laboratory (University of California, San Diego) and were injected into the MSA at a rate of 100 nL/min through a glass pipette using a microsyringe pump under isoflurane anesthesia (induction: 2.5%; maintenance 0.5–2%) using stereotaxic coordinates (+1.0mm A/P, −0.7mm M/L angled at 10º degree towards the midline; 400 nL at −4.8mm D/V; 350 nL at −4.2mm D/V). The pipette was left in place for 5 minutes after the injection before being slowly retracted. Mice were sutured and allowed to recover for a minimum of 7 days.

During a second surgery, mice were implanted with an optic fiber over the medial septal area (MSA, +1 mm A/P, −0.7 M/L, −3.7 D/V, angled at 10° towards the midline) and either a

four-tetrode or eight-tetrode microdrive aimed at the mEC (−0.9 mm A/P from lambda, +3.8 mm M/L, 8° anterior-posterior angle) or dorsal CA1 region of the hippocampus (hippocampus: −1.9 mm A/P from bregma, +1.8 mm M/L). The electrodes initially terminated dorsal to the recording site. Three mice were instead implanted with a 16-channel linear silicon probe (NeuroNexus A1×16-3mm-50-177-CM16LP) in hippocampus. A ground screw was placed over the cortex and the assembly was secured to the skull with anchor screws and dental cement. Postoperative care was administered for five to seven days until mice fully recovered. Initial LFP recordings were performed along with septal stimulation, and any ChR2 mice in which a shift in peak oscillation frequency was not observed (< 20 %) were not trained on the figure-8 maze and were not included in the experiment.

Histological Procedures

Mice were perfused with 0.1 M phosphate-buffered saline (PBS) followed by 4% paraformaldehyde in PBS solution. Brains were post-fixed for 24 hours in 4% paraformaldehyde and then cryoprotected in 30% sucrose solution for 2 days. Brains were then frozen and sliced (40 μm coronal sections for MSA and hippocampus, 40 μm sagittal sections for mEC). Sections were mounted and either coverslipped with Fluoroshield DAPI (Sigma-Aldrich) to visualize fluorophore expression in MSA or stained with cresyl violet and coverslipped with Permount (Fisher Scientific, SP15500) to visualize recording locations in hippocampus and mEC. Slides were imaged using a virtual slide microscope (Olympus, VS120). All entorhinal recordings were histologically confirmed to have been taken from the right mEC (for ChR2 mice: deep and superficial layers in 2 mice, only superficial layer in 5 mice, and only deep layers in 3 mice; quality of histological material did not allow for assignment to cell layer in one mouse). All hippocampal recordings were histologically confirmed to have been taken from the right CA1 area.

Behavior

Mice were trained on a delayed spatial alternation task using a figure-8 maze (50 cm high, 75 cm return and stem arms, 25 cm choice arms, all 5 cm wide). The delay zone was on the first 25 cm of the stem. The room was dimly lit and environmental cues were kept stable. Mice were given a single chocolate sprinkle as a food reward for each correct choice. Food reward was also placed underneath the food reward zone to avoid olfactory guidance. After each animal used the maze, the maze was thoroughly cleaned with water and dish soap. Mice were trained on the task in a series of stages over approximately six weeks. First, mice were habituated to the maze by freely foraging for food for 15 min. Next, mice were trained for three days in a forced alternation task for 40 trials per day. Third, mice were trained to run continuously without barriers for 80 trials until they reaching a criterion of ≥80 % correct for 2 of 3 consecutive days (8±2 sessions). Fourth, delays of 2 s and 10 s were introduced on the central (stem) arm. Mice were trained once daily for 60 trials with an equivalent number of no delay, 2 s delay, and 10 s delay trials until reaching a criterion of ≥80 % correct for 2 of 3 consecutive days (15±5 sessions). They then underwent the implantation surgery. After recovering from surgery, mice were food restricted and retrained on the task to a criterion of 2 out of 3 consecutive sessions at ≥80% correct. Tetrodes were slowly lowered into the cell layer over the course of retraining.

For animals recorded on the track, recordings were performed while animals ran 10–14 laps counterclockwise on a gray rectangular track (150 cm × 50 cm, track width of 10 cm, 3 cm tall guiderails). The rectangular track was placed in the middle of a cue-rich room with a dim light in one corner of the room. Animals were trained daily on the track for a minimum of two days prior to recording.

For the open field mEC recordings, mice (n = 6 after testing in the spatial alternation task and n = 11 without running the spatial alternation task; 8 of those 11 also ran on the rectangular track) were trained to freely forage in a square shaped open field (75 × 75 cm^2) with black walls and a single prominent white cue card along one wall. The open field was placed in the same location for all testing sessions in a room with dim lights and distal cues along all walls. Mice were habituated to the open field for several days before recordings and optogenetic stimulation. Once trained, each mouse performed at least three sessions per day: one baseline recording session without optical stimulation, one to three stimulation sessions (8, 10, or 12 Hz randomized), and one final baseline recording session.

Electrophysiological Recordings

Tetrodes each consisted of four 17 μm platinum-iridium (90/10 %) wires (California Fine Wire Company) and were assembled into a microdrive. Electrode tips were plated with platinum to reduce impedance to 150–250 kΩ at 1 kHz. The microdrive was connected through a multichannel, head-mounted preamplifier to a digital Neuralynx recording system (Neuralynx, Bozeman, MT). A pulley system counteracted the weight of the tether and headstage. Continuous LFP was recorded from each tetrode by band-pass filtering (0.1–900 Hz) and sampling at 32 kHz. Position and head-direction data were obtained from a red and a green LED located on either side of the preamplifier by sampling at 30 Hz with a camera mounted above the experimental area. Signals from each tetrode wire were amplified (5,000–20,000x) and band-pass filtered to either record LFP (1–900 Hz) or spikes (0.6–6 kHz). Spike waveforms above 35–45 μV were time-stamped and digitized at 32 kHz for 1 ms.

Optic Stimulation

Light was delivered to the implanted optic fiber (Thor Labs, 0.50 NA multimode fiber, 230 μm diameter, 200 μm core, 4 mm long, sanded) using a 473 nm Blue DPSS Laser System and an optic fiber patch cord (Doric Lenses, 200 μm core, 0.22 NA). Control green light was delivered using a 532 nm Green DPSS Laser. The output intensity was adjusted to between 9.0 and 12.0 mW, and the light was pulsed with a 50 % duty cycle at the desired stimulation frequency. In the spatial alternation task, each subject was tested once per day in 6 blocks of 10 trials with two sets of delay conditions (no delay, 2 s, 10s) and stimulation on/off on alternating blocks. Restricting stimulation to different regions of the maze was done by passing the × and y coordinates from the Neuralynx Cheetah system to MATLAB, version 2015b. A custom MATLAB script processed the x-y coordinates and turned rhythmic stimulation on once animals entered the targeted zone and off once the animal exited the zone.

Single Unit Identification

Single-units were manually isolated offline using MClust 3.5 and MATLAB 2009b (Redish, A.D., http://redishlab.neuroscience.umn.edu/MClust/MClust.html). Neurons were separated in two-dimensional space based on the peak amplitude, peak-to-valley amplitude, and energy of spike waveforms. Based on plotting the mean firing rate against the peak-valley ratio, we determined that a rate cutoff of 15 Hz separated putative mEC principal cells from putative mEC interneurons and that a combined cutoff of 10 Hz and a peak-to-valley ratio of 1.5 separated putative hippocampal principal cells from putative hippocampal interneurons (Extended Data Fig. 1b). The same cells were tracked within each day but were not recorded across days. Cells that were not present or not clearly isolated in any sessions of the day were not included in the analysis. All cells used for further analysis had stable and well-isolated clusters based on L-ratio values and isolation distance (Extended Data Fig. 1c and d).

Spatial Analyses on the rectangular track

Positions on the rectangular track were linearized into 116 bins (3.5 cm per bin) for analysis of spatial properties. Rate maps were then computed as the number of spikes per time spent in each spatial bin and were smoothed by a pseudo-Gaussian kernel with a standard deviation of 1 bin. Spatial information was calculated as,

$$I = \sum p_i \cdot \frac{F_i}{F} \cdot \log \frac{F_i}{F}$$

where I is the spatial information in bits/spike, p_i is the probability of occupancy in bin I, F_i is the mean firing rate for bin I, and F is the mean firing rate. We calculated the correlation between rate maps for the 1st half of trials compared to the 2nd half of trials to quantify the rate map stability. Place fields were defined as cells that had a peak spatial firing rate greater than 5 Hz and that maintained > 20 % of their peak rate for at least 20 cm and less than 140 cm.

Spatial analyses in the open field

Rate maps.—The recording box was divided into 3 × 3 cm bins. Firing rate maps were constructed by dividing the total number of spikes in each bin by the total time the animal spent in the same bin. Rate maps were smoothed with a 5 by 5 pixel filter [0.0025 0.0125 0.0200 0.0125 0.0025; 0.0125 0.0625 0.1000 0.0625 0.0125; 0.0200 0.1000 0.1600 0.1000 0.0200; 0.0125 0.0625 0.1000 0.0625 0.0125; 0.0025 0.0125 0.0200 0.0125 0.0025], and bins that were more than 2.5 cm away from any tracked path or had a total occupancy of less than 150 ms were assigned NaNs in the rate map.

Grid score and spatial auto-correlation.—Grid cells were identified by calculating a gridness score as described previously[26,58]. Briefly, rate maps with 1.5 cm × 1.5 cm bin size were used to generate a spatial auto-correlation matrix, from which an annulus that contained the first set of peaks around the center, but excluded the central peak was extracted. Spatial correlations of the annulus with rotated versions of itself were then performed in 30° steps. If there is six-fold symmetry, correlations at 30, 90 and 150°

would be low, whereas correlations at 60, 120, 180° would be high. The gridness score was calculated as the difference between the average of the first and the average of the second set of rotation values.

Head-direction score.—The head direction of the animal was calculated from the angle between the two diodes in the horizontal plane[26]. The number of spikes within each 1° angular bin was divided by the time spent at that angle to generate polar plots. The mean vector length of these plots was defined as the head direction score.

Speed score.—Speed cells were classified based on speed scores[37], which were obtained by calculating the Pearson product-moment correlation between the cells' firing rate and the instantaneous running speed in 33 ms bins (corresponding to the acquisition rate of position data). Firing rates were smoothed with a 250 ms wide Gaussian filter, and instantaneous running speed was obtained using a Kalman filter on the position data.

Cell type identification.—Classification of a cell as either a grid, head direction, or speed cell was performed by determining whether the respective score was greater than the 95th percentile of the scores from shuffled data. Shuffled spike trains for each cell were generated by randomly selecting a value between 20 s and 580 s and by then adding the value to the timestamp of each spike. Spike times exceeding the total duration of a session were wrapped to the beginning of each session. Shuffling was repeated 1000 times for each cell in each session, and values from the shuffles were pooled across cells. In addition, head direction cells were further sub-classified into narrow and broad HD cells based on the finding that there was a clear cluster of narrowly tuned cells with scores > 0.5. Because each cell was recorded for at least three sessions (stimulation as well as baseline before and after stimulation), we had to account for the possibility that a cell was not consistently classified across sessions. To assign a cell to a particular functional cell type, we therefore required that the respective score was above the 95th percentile pooled cutoff in at least two of all recorded sessions in a day.

Single-cell FFT analyses

For each cell, spike times were first binned at a sampling rate of 500 Hz. The temporal autocorrelation between spike times was calculated from the resulting vector. The power spectrum of the temporal autocorrelation was obtained via the Chronux function mtspectrumc() using a padding factor equal to six powers of 2 over the sample size. The single-cell frequency was then taken as the frequency with maximum power in the 6–14 Hz range.

LFP Analysis

For each session, the LFP from the tetrode with the highest mean power between 6 and 10 Hz was selected for analysis. The raw LFP signal was down-sampled to 2 kHz, and power at all frequencies was calculated by performing an FFT, using the Chronux function mtspecgramc() with the following parameters: Window Size = 10s, Window step = 5 s, Number of tapers = 5, Time-window product = 3. Because analysis restricted to maze segments included short time segments, a wavelet-based method was more appropriate.

Therefore, power at all frequencies in specific zones of the maze during the spatial alternation task was calculated using a Morlet wavelet of width 6. The time-frequency spectrograms that were obtained using the wavelet method were then normalized to account for the 1/f noise in trials when there was no light stimulation.

Current source density analysis

This analysis was implemented as described and validated previously[59, 60]. Using the depth profile of the recordings with 16-channel silicon probe during periods without light stimulation, we assigned the channel with the highest sharp-wave ripple (SWR) amplitude during rest periods to the CA1 stratum pyramidale (sp) based on visually confirming SWR presence and amplitude. The channel with the most prominent sink-source during running was identified as being placed in the stratum lacunosum moleculare (slm). The raw LFP from this channel was filtered between 6–14 Hz, and peaks in this filtered signal were detected. A peak was identified as the local maximum in the filtered signal that was >2 standard deviations above the mean absolute signal. Segments of the raw LFP signal on each channel along the depth of the shank were subsequently aligned with reference to the peak. The differential between successive average aligned channels was used to generate the CSD profile.

Quantification of pacing scores

To estimate how effectively the optogenetic stimulation could override endogenous theta oscillations, we calculated a pacing score (Extended Data Fig. 1a). LFP from the tetrode with the highest theta power was used to calculate the spectral power across time for frequencies between 6–14 Hz. We reasoned that effective stimulation would lead to a consistent peak frequency within a narrow band, whereas endogenous theta oscillations would have peak frequencies dispersed over a broader range. Therefore, the recording period was divided into 2 s long segments and the peak oscillation frequency was measured in each segment. A histogram of the distribution of peak frequencies was generated for periods with and without stimulation, and the pacing score was defined as the highest proportion in a narrow frequency band (i.e., 0.2 Hz bin width within 1 Hz of the stimulation frequency) during periods with stimulation (see Extended Data Figs. 1, 7 and 8). This method was chosen because a previously used pacing score[19], which is based on the ratio of power within 1 Hz of the stimulation frequency and power at the endogenous theta frequency (7–9 Hz) was not suitable for estimating pacing at 8 Hz. We compared the values that were obtained with the previous ratio-based score with the current proportion-based score and found that the two types of scores were highly correlated (Extended Data Fig. 7e).

Quantification of viral vector expression

All cre-dependent viral vectors included a fluorophore and sections throughout the MSA were examined for fluorophore expression. The sections were imaged using a virtual slide microscope (Olympus, VS120) at 10x magnification. Three or five sections (0.20 mm or 0.12 mm apart) along the antero-posterior extent of the MSA were analyzed using Fiji ImageJ. In these sections, regions of interest were drawn around cells and fibers with fluorophore expression in the medial septum and diagonal band of Broca in each hemisphere. The estimated volume of opsin expression in MSA was then calculated by

adding the areas across sections and by multiplying by the distance between sampled sections. In addition, all volume measurements were corrected for the total AP distance of the MSA (1 mm) compared to the sampled AP distance (0.6 mm when either 3 or 5 sections were sampled). Using the same procedures for the quantification of expression volume, the histological material from 10 mice in a previously published study[19] was re-quantified and is shown for comparison in Extended Data Fig. 7a and b. Loss or damage of tissue during histological processing precluded quantification in four mice with ChR2 expression in MSA. These mice could thus not be included in any analyses by expression volume, but their pacing scores (P13: 0.20, P125: 0.48, P127: 0.36, P129: 0.21; Extended Data Fig. 1) were well within the range of mice with confirmed expression volumes.

LFP-spike phase coupling

We used a waveform-based estimation of instantaneous theta phase[61]. For the tetrode with the highest theta power, the LFP was bandpass filtered between 6–20 Hz and used to find peaks, troughs, and zero crossings. Theta peaks were defined as 0 degrees, troughs as 180 degrees, and zero crossing as 90 and 270 degrees. We then interpolated phase values between these reference points to determine the each spike's phase with respect to the LFP. Theta modulation strength (also referred to as spike phase locking) for each cell was defined as the mean resultant length of the distribution of firing phases.

Statistics

All statistics were done using built in MATLAB (R2019b) functions. No statistical tests were used for predetermining sample sizes, but our sample size is similar to other studies or exceeds the sample size of previous studies (e.g., ~25 mice for key behavioral comparisons, >500 cells for key mEC recordings). KS tests were performed to examine normality. If normality could be assumed, we used paired two-tailed t-tests. If normality could not be assumed, nonparametric statistics were performed (Kruskal-Wallis, Friedman, and Wilcoxon tests). The behavioral experiments were designed to include blocks of light stimulation that alternated with blocks without stimulation, such that day-to-day variability in behavioral performance could be controlled for by taking the difference between blocks with and without stimulation. Stimulation frequencies were randomized across days. All comparisons were therefore done using paired comparisons and p values were corrected with the Holm-Bonferroni method to correct for repeated testing at multiple stimulation frequencies. The statistics for the recordings in the open field and for behavioral testing in the spatial alternation task are described in detail in Supplementary Tables 1–3. Data collection and analysis were not performed blind to the conditions of the experiments. Criteria for excluding data points from the analysis (e.g., low pacing scores), along with the rationale for exclusion, are stated throughout the Methods, Results, and figure legends.

Data availability

The data for all recordings are available at datadryad.org (https://doi.org/10.6076/D1MK58)[59]. All other data that support the findings of this study are available from the corresponding author upon request.

Code availability

The code for analyzing the recordings is available at datadryad.org (https://doi.org/10.6076/D1MK58)[59]. All other data that support the findings of this study are available from the corresponding author upon request.

Extended Data

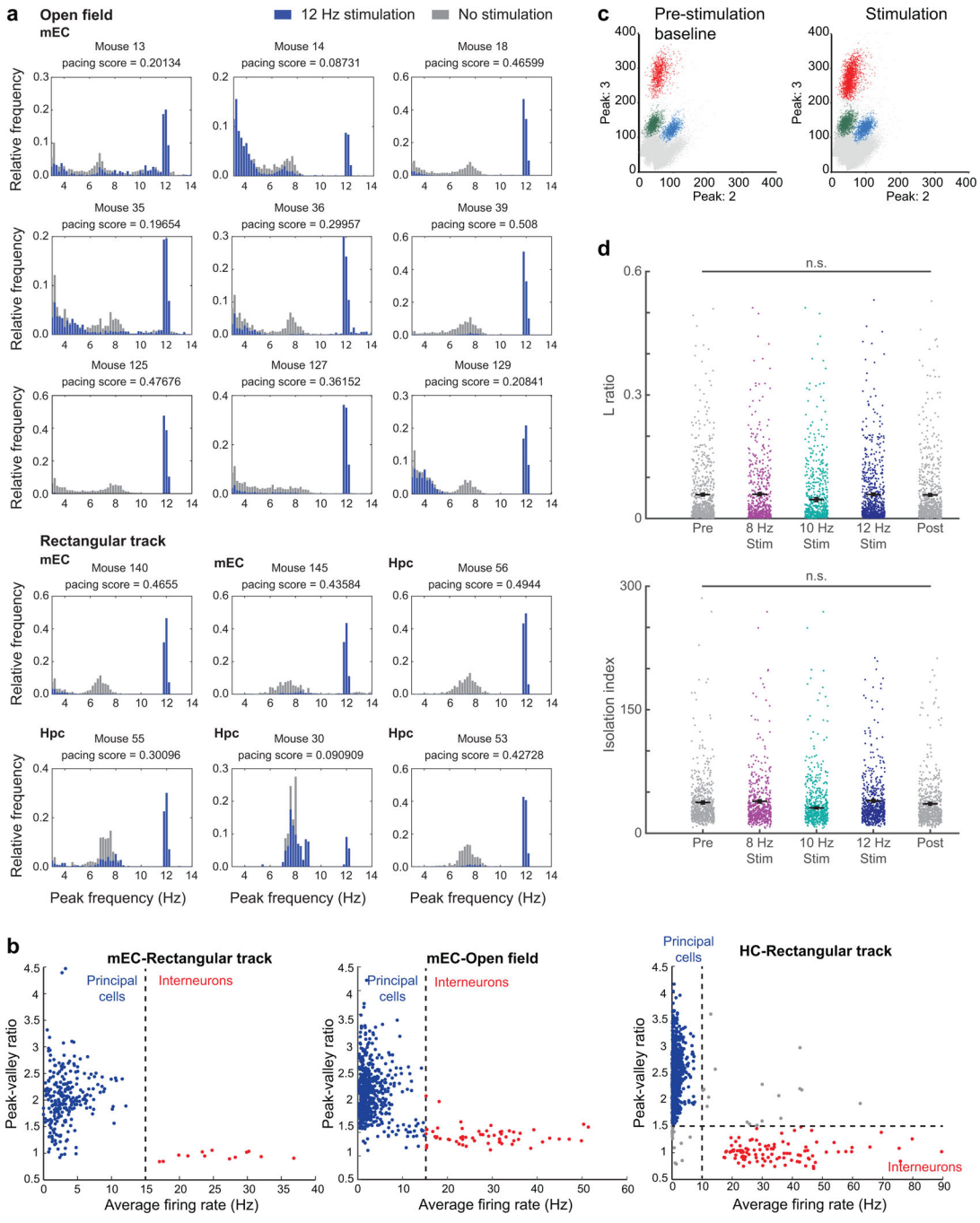

Extended Data Fig. 1. LFP pacing efficiency and single unit identification.

(**a**) Pacing efficiency scores for recordings when each mouse explored the open field (*top*) or rectangular track (*bottom*). For every 2-s time-window, the peak LFP frequency was calculated for sessions without stimulation (*gray bars*) and with 12 Hz stimulation (*blue bars*), and the probability distribution of these peak LFP frequencies was plotted for each animal. Efficient pacing results in a narrow frequency peak at the stimulation frequency, and the pacing efficiency score was therefore defined as the maximum probability (in 0.2 Hz wide bins within 1 Hz of the stimulation frequency) in stimulation sessions. (**b**) The ratio of the spike waveform peak to trough amplitude (peak-valley ratio) and average firing rate (Hz) for each recorded cell was calculated to determine appropriate cutoff thresholds that separated between putative principal cells (*blue circles*) and putative interneurons (*red circles*). For cells recorded from the mEC either on the rectangular track (*left*) or the open field (*middle*), we used a rate cutoff of 15 Hz. For cells recorded from the hippocampus (*right*), we used a combined rate cutoff of 10 Hz and peak-valley cutoff of 1.5. (**c**) Example of multiple single-unit clusters recorded during the pre-stimulation baseline (baseline 1, *left*) and during optical stimulation (*right*). Defined single-unit clusters (*red, green and blue*) remained stable between sessions without stimulation and with stimulation. (**d**, *top*) L-ratio calculated for clusters of single units recorded in the mEC. (**d**, *bottom*) Isolation distance values calculated for clusters of single units recorded in the mEC. There was no change in L-ratio [n(B1, 8 Hz, 10 Hz, 12 Hz, B2) = 593, 476, 111, 531, 593 cells from 11 mice, H(4, 2299) = 2.17, P = 0.704, Kruskal-Wallis test] or isolation distance [n(B1, 8 Hz, 10 Hz, 12 Hz, B2) = 580, 462, 109, 518, 579 cells from 11 mice, H(4, 2243) = 7.91, P = 0.095, Kruskal-Wallis test] across stimulation conditions. n.s., not significant.

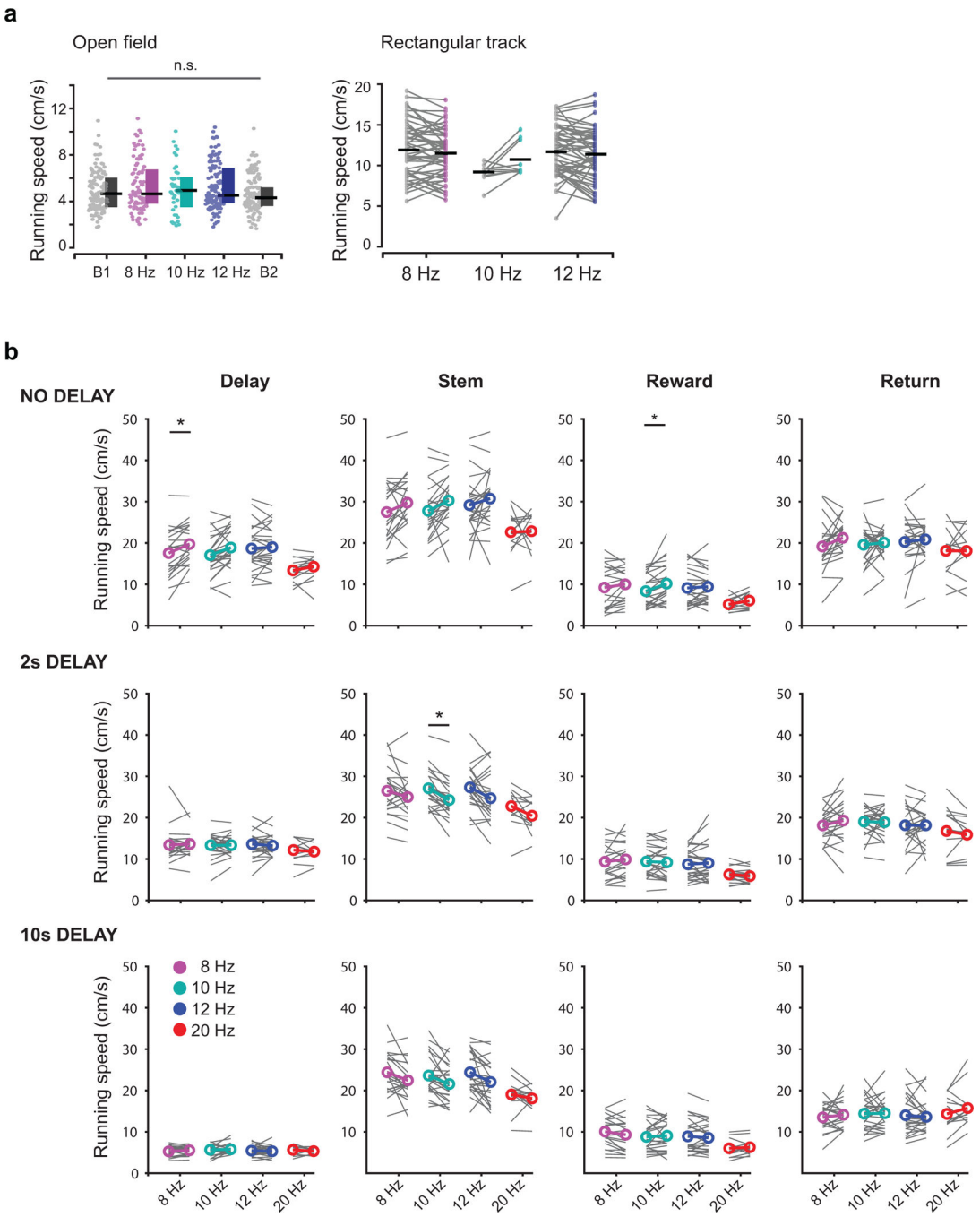

Extended Data Fig. 2. Running speed during periods with and without MSA stimulation.

(**a**) Running speed in either the open field (*left*) or on the rectangular track (*right*) was not altered when oscillations were paced by MSA stimulation [open field: grey and colored dots are individual data points, horizontal bars are medians, top and bottom of boxes are 25th and 75th percentile, $n = 11$ mice, $H(4,487) = 7.2$, $P = 0.13$, Kruskal Wallis test; linear track, grey and colored dots are individual data points, baseline vs stimulation, 8 Hz: $n = 55$ sessions in 6 mice, mean (±SEM), 12.08 (±0.44) and 11.51 (±0.40), $t(54) = 2.31$, $P = 0.025$ (0.074, Holm-Bonferroni corrected); 10 Hz: $n = 9$ sessions in 3 mice, median (25th, 75th percentile),

9.31 (8.77, 9.56) and 9.40 (9.33, 12.44), $W(10) = 37$, $P = 0.065$; 12 Hz: $n = 54$ sessions in 6 mice, mean (±SEM), 11.87 (±0.41) and 11.36 (±0.43), $t(53) = 1.67$, $P = 0.10$, two-sided paired t-test for normally distributed data, otherwise two-sided Wilcoxon signed rank test]. n.s., not significant. (**b**) There were no consistent effects on running speed in any of the maze zones during light stimulation in the spatial alternation task. During no delay trials, there was a minor increase in the delay zone with 8 Hz stimulation (note that the mice are running through the delay zone in the no delay trials) and in the reward zone with 10 Hz stimulation [delay, 8 Hz: $n = 22$ mice, $z = -3.13$, $P = 0.0017$ (0.027, Holm-Bonferroni corrected); reward, 10 Hz: $n = 25$ mice, $z = -3.11$, $P = 0.0019$ (0.028, Holm-Bonferroni corrected), two-sided Wilcoxon signed rank tests]. In 2 s delay trials, there was a minor decrease in running speed with 10 Hz stimulation on the stem [$n = 25$ mice, $z = 3.92$, $P = 9.0 \times 10^{-5}$ (0.0014, Holm-Bonferroni corrected), two-sided Wilcoxon signed rank test]. For all other comparisons, we do not find any differences in running speed on any of the maze segments.

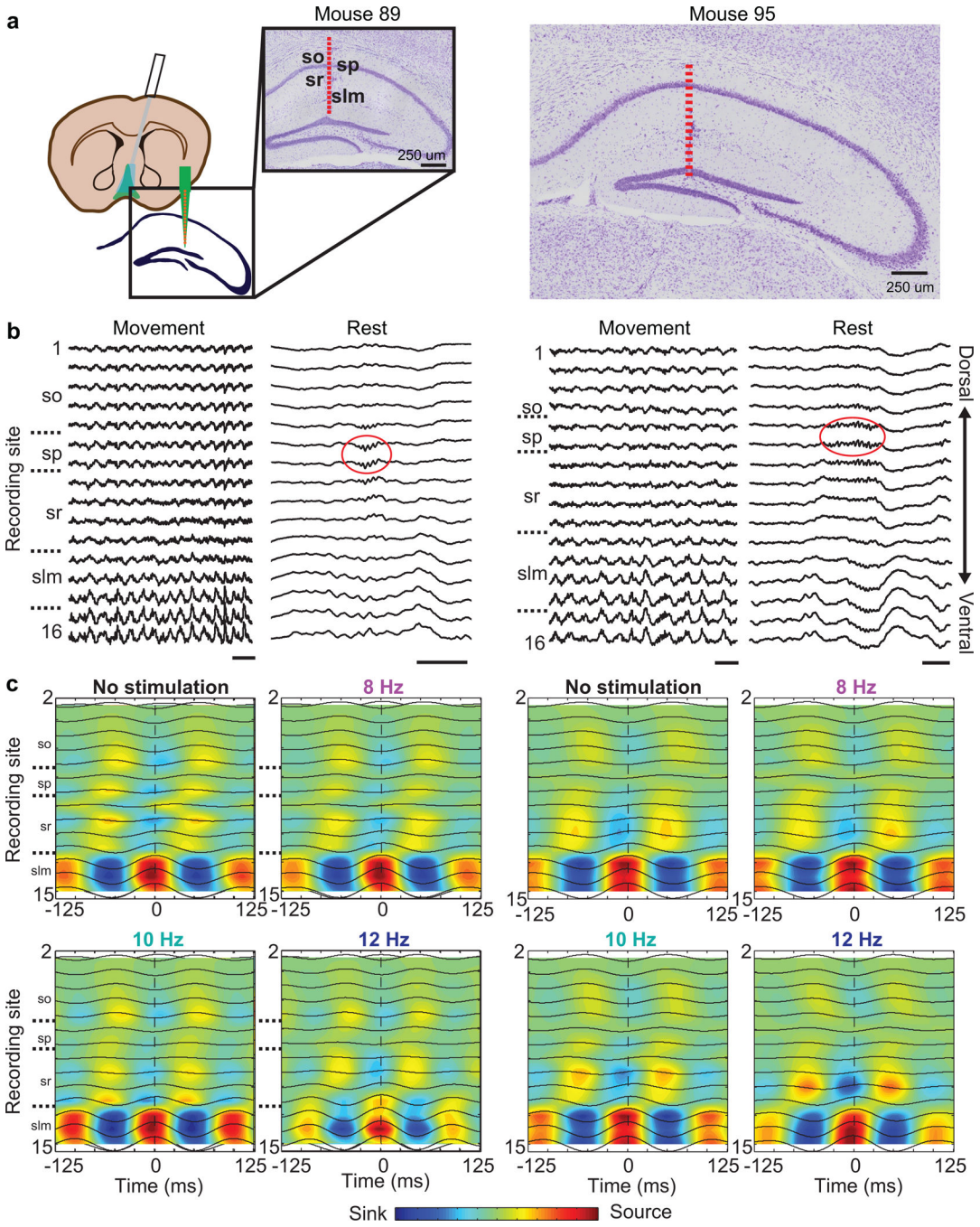

Extended Data Fig. 3. The hippocampal depth profile during paced oscillations corresponded to the depth profile during endogenous theta oscillations.

(**a**) Sixteen-site linear silicon probes were chronically implanted in the hippocampus, and LFP recordings were performed in freely moving mice (n = 3 with one mouse excluded from analysis because of inadequate pacing; average pacing efficiency scores: 0.37 for mouse 89, 0.16 for mouse 95, and 0.04 for the excluded mouse 97). Schematic and brightfield histology images of the dorsal hippocampus for mouse 89 and 95. (**b**) Example raw LFP traces from all 16 recording sites during movement and rest. Ripple amplitude is known

to be maximal in the pyramidal cell layer (encircled with red line), and alignment of the probe with the pyramidal layer was performed by visual inspection of sharp wave ripple amplitude and matched with the position of the probe in the histological reconstruction in (a). Scale bar is 250 ms. (**c**) Average current source density across hippocampal layers from recordings without stimulation (no stimulation) and with rhythmic stimulation at 8, 10, and 12 Hz. Periods from −125 to +125 ms are shown to include approximately two theta cycles (mouse 89, *first and second column*; mouse 95, *third and fourth column*). Note that there is a shortening of the theta cycle with higher stimulation frequencies, but during periods with stimulation the most pronounced current source-sink pair remained in slm, which is the termination zone of direct projections from entorhinal cortex. The distribution of less pronounced sink-source pairs across other hippocampal layers is also consistent between stimulation and no stimulation sessions. so, stratum oriens; sp, stratum pyramidale; sr, stratum radiatum; slm, stratum lacunosum moleculare.

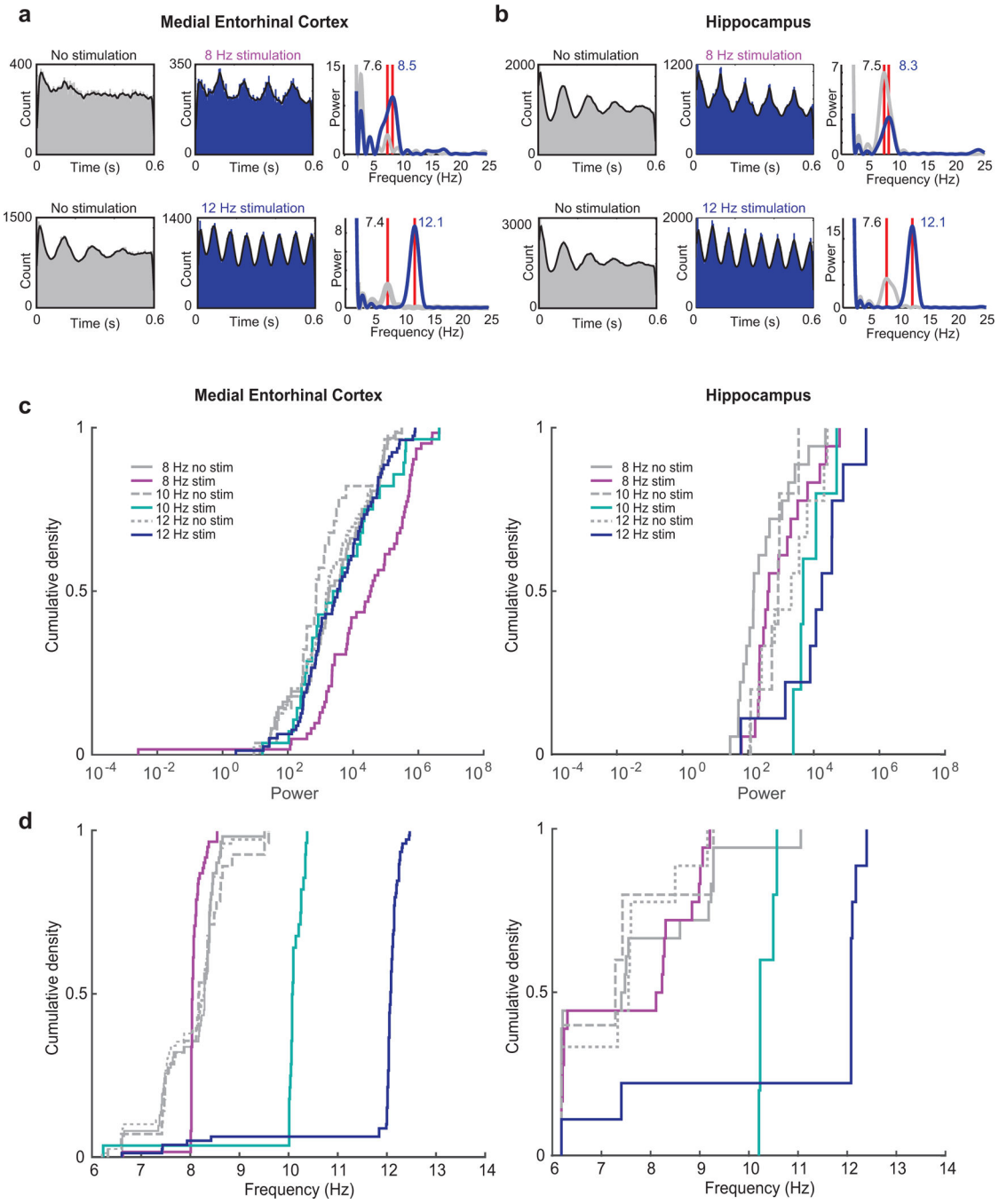

Extended Data Fig. 4. mEC and hippocampus interneurons shifted their intrinsic firing frequencies.

(**a**) Example spike time autocorrelations for mEC interneurons during periods without stimulation (gray, *left*) and with stimulation (blue, *middle*) at 8 and 12 Hz. *Right*, FFT analysis of spike trains shows accelerated frequencies during stimulation compared to no stimulation sessions. Red vertical lines denote the peak oscillation frequency without and with light stimulation. (**b**) Same as in (a) but for hippocampal interneurons in the CA1 area. (**c**) Cumulative distribution function of the peak power (from the FFT analysis of

spike trains) for mEC interneurons (*left*) and hippocampal interneurons (*right*). Interneurons generally showed high amplitude theta modulation at baseline, and a further increase compared to baseline was only observed at a subset of stimulation frequencies (mEC, 8, 10 and 12 Hz: $K = 0.50, 0.30, 0.16$; $P = 1.7 \times 10^{-5}$, 0.20, 0.44; hippocampus, 8, 10, and 12 Hz: $K = 0.50, 0.80, 0.56$, $P = 0.014, 0.036, 0.078$, two-sided KS tests). (**d**) Cumulative distribution function of the peak oscillation frequency of mEC interneurons (*left*) and hippocampal interneurons (*right*). Interneurons in mEC and hippocampus were similarly entrained [8, 10, and 12 Hz stimulation, mEC: $n = 43, 23, 57$; difference between stimulation frequency and cells' oscillation frequency, median (±iqr) = 0.04 (±0.08), 0.10 (±0.23), 0.09 (±0.16); hippocampus: $n = 18, 5, 9$; median (±iqr): 0.19 (±2.64), 0.25 (±0.29), 0.11 (±1.21); mEC vs hippocampus: $z = -0.14, -2.04, -0.36$, $P = 0.89, 0.04, 0.72$, two-sided Wilcoxon rank sum tests].

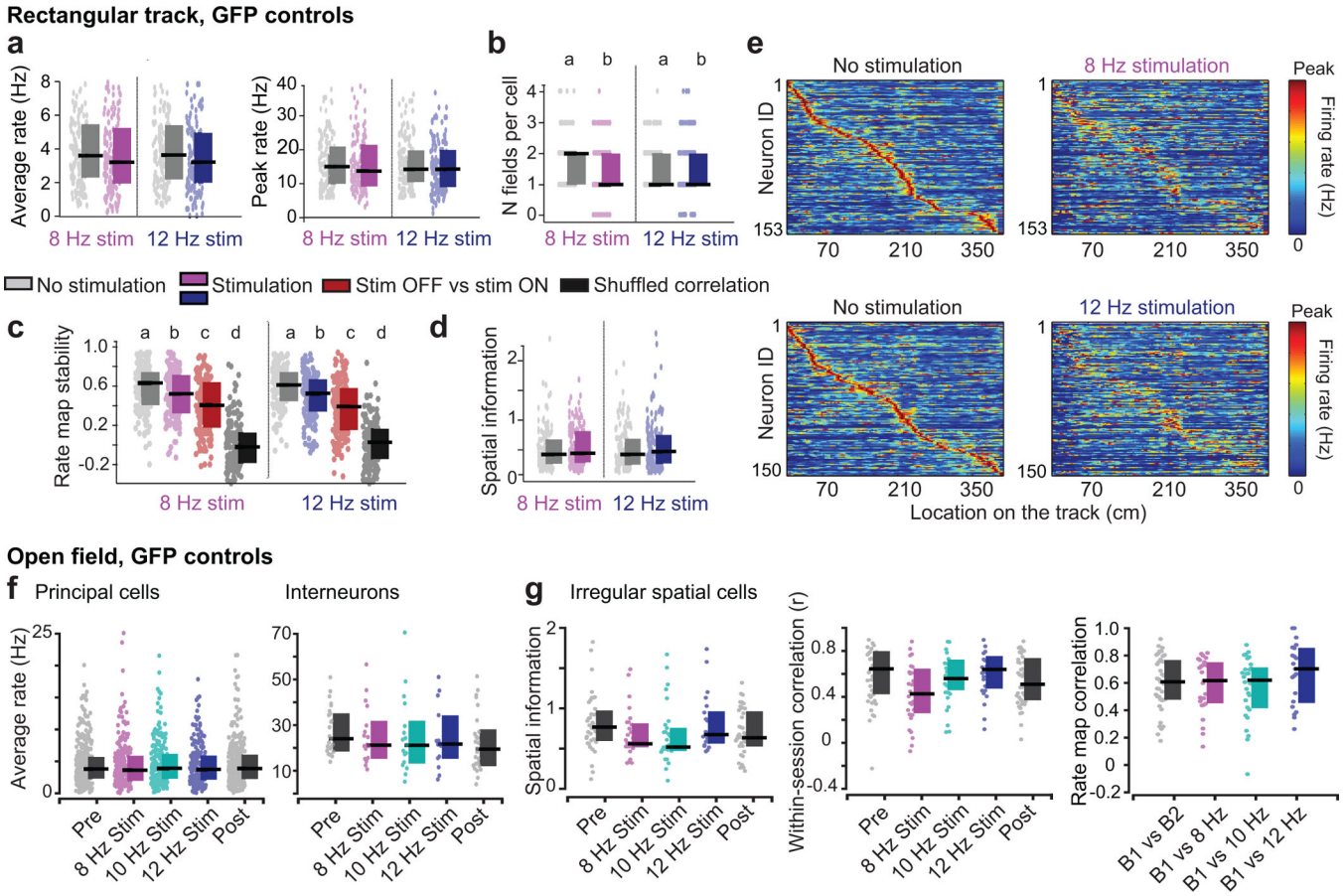

Extended Data Fig. 5. Light-induced remapping was observed in the mEC of control mice on the rectangular track, but not in the open field.

(**a**) **Rectangular track**, Firing statistics of mEC cells in GFP control mice ($n = 6$) expressing mEmerald in the medial septal area. As described for Fig. 5, the mice ran on a rectangular track with alternating light-off and light-on laps. During light on laps, stimulation frequency was either 8 Hz or 12 Hz. The mean firing rate and peak firing rate of principal cells did not differ between no stimulation and stimulation laps for either stimulation frequency [Average firing rate, 8 and 12 Hz: $n = 153$ and 150 cells, two-way

ANOVA, stim frequency*light-off vs on, interaction, $F(1,602) = 0.037$, $P = 0.85$, stim frequency, $F(1,602) = 0.10$, $P = 0.76$, light-off vs on, $F(1,602) = 2.83$, $P = 0.093$. Peak firing rate, 8 Hz and 12 Hz: $n = 153$ and 150 cells, two-way ANOVA, stim frequency*light-off vs on, interaction, $F(1,602) = 0.15$, $P = 0.70$, stim frequency, $F(1,602) = 0.79$, $P = 0.37$, light-off vs on, $F(1,602) = 0.03$, $P = 0.86$]. (**b**) A decrease in the number of place fields per cell as a result of light-induced remapping was observed across both stimulation frequencies in control mice [8 Hz and 12 Hz: $n = 153$ and 150 cells, two-way ANOVA, stim frequency*light-off vs on, interaction, $F(1,602) = 0.28$, $P = 0.60$, stim frequency, $F(1,602) = 1.54$, $P = 0.21$, light-off vs on, $F(1,602) = 10.6$, $P = 0.0012$]. Letters above columns (a, b) indicate significant differences between light-on and light-off conditions, two-sided Tukey-Kramer posthoc tests. (**c**) Light delivery in GFP control mice resulted in a significant decrease in place field stability within light-on trials and resulted in remapping, measured as the correlation between light-on and light-off trials. Both measures remained higher than a shuffled distribution suggesting partial light-induced remapping. There were no differences between stimulation frequencies for rate map stability condition [within light-off, within light-on, between light-on and light-off, shuffled; 8 and 12 Hz: n = 153 and 150 cells, two-way ANOVA, stim frequency*condition, interaction, $F(3,1201) = 0.29$, p = 0.83, stim frequency, $F(1,1201) = 0.35$, p = 0.56, condition, $F(3,1201) = 328.2$, $p < 0.001$]. Different letters (a-d) above columns indicate significant differences ($P < 0.001$) between conditions, two-sided Tukey-Kramer posthoc tests. (**d**) There was no change in spatial information of mEC fields on the linear track despite significant remapping [8 Hz and 12 Hz: n = 153 and 150 cells, two-way ANOVA, stim frequency*light-off vs on, interaction, $F(1,602) = 0.26$, $P = 0.61$, stim frequency, $F(1,602) = 0.04$, $P = 0.84$, light-off vs on, $F(1,602) = 3.18$, $P = 0.075$]. (**e**) Positions of the spatial fields of mEC principal cells on the rectangular track are linearized and ordered left to right for each stimulation frequency according to the position during light-off sessions. The reorganization across light-off and light-on trials arises as a result of blue light delivery in control mice without pacing. (**f**) **Open field**, MEC cells were recorded from GFP control mice ($n = 6$) in a random foraging task, as described in Fig. 6. Light delivery (at either 8 Hz, 10 Hz, or 12 Hz) was performed during 1–2 sessions in-between two baseline sessions without light delivery. There was no change in the mean firing rate of principal cells and interneurons during stimulation sessions. (**g**) Light stimulation did not have consistent effects on irregular spatial cells as measured by the spatial information, spatial field stability (within-session correlation), and the extent of remapping (rate map correlation across sessions) [n(B1, 8Hz, 10 Hz, 12 Hz, B2) = 39, 27, 29, 21, 39 cells from 6 mice]. In (a-d), (f), and (g), grey and colored dots are individual data points, horizontal bars are medians, top and bottom of boxes are 25th and 75th percentile, see Supplementary Table 2 for detailed statistics.

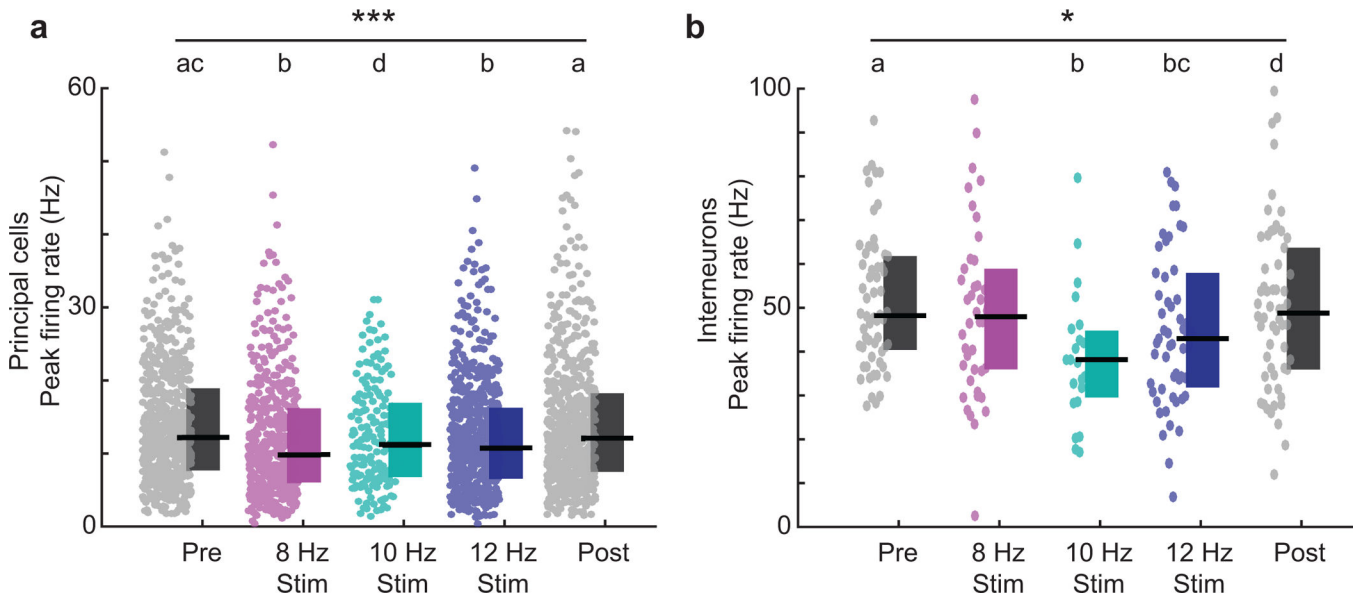

Extended Data Fig. 6. Peak firing rates of mEC cells during MSA stimulation.

(**a**) There was a minor decrease in the peak firing rate of principal cells during MSA stimulation compared to baseline (grey and colored dots are individual data points, horizontal bars are medians, top and bottom of boxes are 25th and 75th percentile). Peak rate with 8 and 12 Hz stimulation was decreased compared to both the pre- and post-stimulation baseline. Peak rate at 10 Hz was decreased only compared to the pre-stimulation baseline [n(B1, 8 Hz, 10 Hz, 12 Hz, B2) = 593, 477, 170, 589, 592 cells from 11 mice, H(4,2416) = 32.09, $P = 1.8 \times 10^{-6}$, Kruskal Wallis test]. (**b**) There was a significant decrease in the peak firing rate of interneurons during 10 Hz and 12 Hz stimulation sessions compared to the pre-stimulation baseline (grey and colored dots are individual data points, horizontal bars are medians, top and bottom of boxes are 25th and 75th percentile). The rates with 12 Hz stimulation also differed from the post-stimulation baseline [n(B1, 8 Hz, 10 Hz, 12 Hz, B2) = 58, 42, 23, 55, 58 cells from 11 mice, H(4,231) = 12.04, $P = 0.017$, Kruskal Wallis test]. *** $P < 0.001$, * $P < 0.05$, see Supplementary Table 2 for detailed statistics.

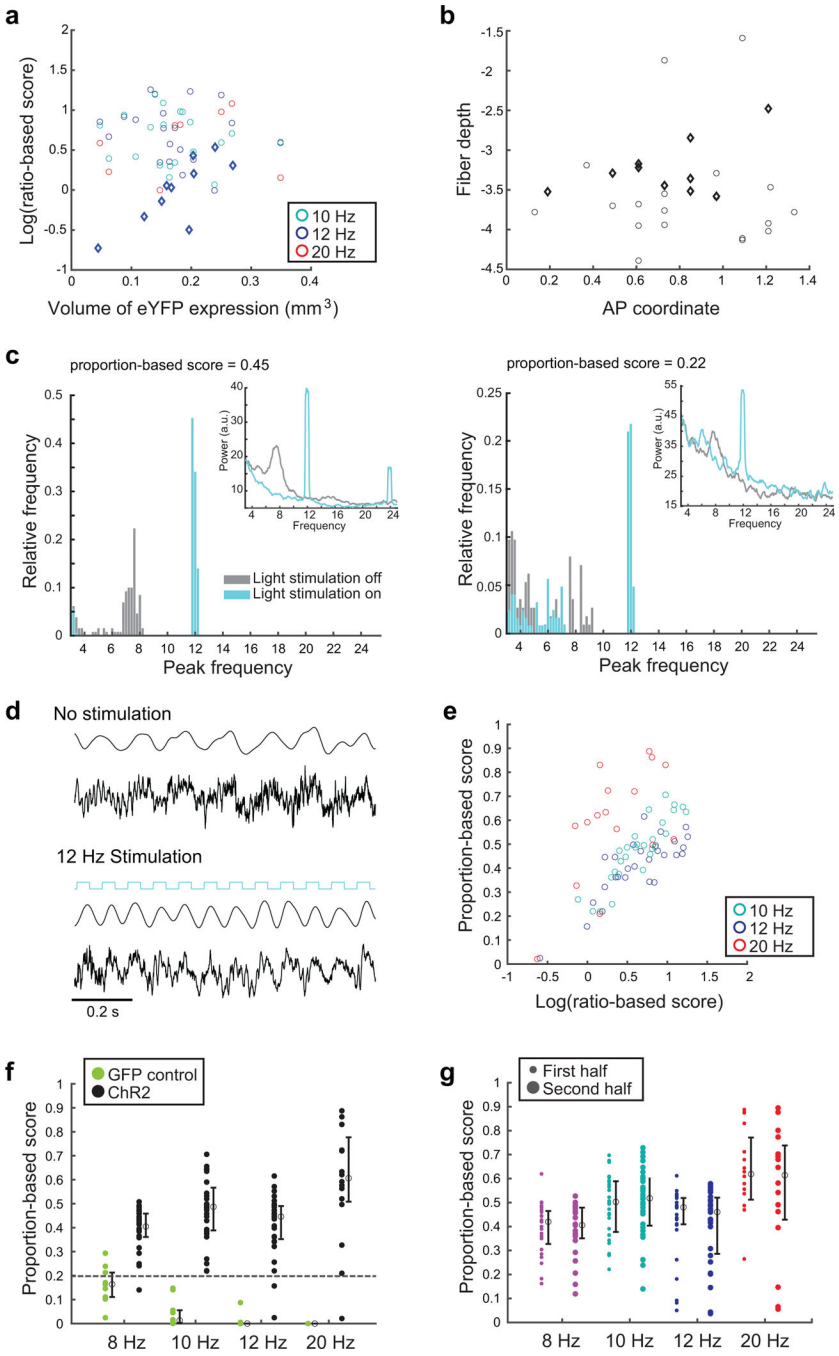

Extended Data Fig. 7. Pacing was efficient for all mice that were included in analysis of behavioral data.

(**a**) Volume of opsin expression in MSA (i.e., medial septal area and diagonal band of Broca) is plotted against the log of the ratio-based score during 10 Hz, 12 Hz, and 20 Hz stimulation (*open circles*). Our previously published data (Fig. 1d in ref. 19) which showed a correlation between expression volume and pacing scores, are plotted for comparison (*diamonds*), but with expression volume re-quantified to match the methods of the current study. The previously reported correlation between expression volume and pacing efficiency was not observed in the current dataset [ratio-based score: n(10 Hz, 12 Hz, 20 Hz) = 28,

28, 16 mice, *rho* = −0.016, −0.092, 0.27, $P = 0.94, 0.64, 0.32$; proportion-based score: n(8 Hz, 10 Hz, 12 Hz, 20 Hz) = 25, 28, 28, 16 mice; *rho* = 0.075, 0.064, −0.36, −0.29; $P = 0.72, 0.75, 0.058, 0.28$, Spearman rank correlations). In the current dataset, pacing scores were consistently high, and it is possible that the correlation is not evident without including a sufficient number of cases with low scores. (**b**) Some mice in (a) showed high pacing efficiency with relatively low expression volumes which may be a consequence of differences in fiber placement in the current study (*open circles*) compared to the previous study (ref. 19, *diamonds*). (**c**) The previously used ratio-based pacing score (power within 1 Hz of the stimulation frequency divided by power at 7–9 Hz) was not designed to capture pacing efficiency with 8 Hz stimulation. To use a score that can be applied to all frequencies, we therefore considered the observation that efficient pacing results in a narrow frequency distribution around the stimulation frequency. To quantify the frequency distribution, we first measured the predominant LFP oscillation frequency during every 2 second interval and binned these measurements with a 0.2 Hz resolution. The peak proportion (i.e., relative frequency) in bins within 1 Hz of the stimulation frequency is taken as the proportion-based pacing efficiency score. Histograms and the corresponding power spectra (*inserts*) show that pacing was highly efficient for scores >0.2 (examples with scores of 0.45 and 0.22 are shown). (**d**) Filtered (3–22 Hz, *top*) and raw traces (*bottom*) during periods with and without stimulation show efficient pacing of the hippocampal LFP. Traces are from the session for which pacing efficiency is shown to the left in (c). Light pulses are shown as a *blue line*. (**e**) For frequencies higher than 8 Hz, where both the ratio-based and the proportion-based scores can be used, the scores are highly correlated [n(10 Hz, 12 Hz, 20 Hz) = 29, 29, 17 mice, *rho* = 0.90, 0.78, 0.53, $P = 4.7 \times 10^{-7}$, 2.6×10^{-6}, and 0.029; Spearman rank correlations after confirming with two-sided KS tests that scores were not normally distributed]. (**f**) Pacing was highly efficient for most animals and stimulation frequencies [n(8 Hz, 10 Hz, 12 Hz, 20 Hz) = 25, 29, 29, 17 ChR2 mice and 10, 10, 10, 6 GFP mice]. Dots are individual data points, open circles and bars are median ± 25th to 75th percentile. When mice with opsin expression did not reach a score of 0.2 (*stippled line*) at a particular stimulation frequency, the behavioral data at the frequency were excluded from the analysis (n = 1 at 8 Hz, 2 at 12 Hz, and 1 at 20 Hz). A score of 0.2 was not exceeded in any of the GFP controls except for three cases at the 8 Hz frequency. At the 8 Hz frequency, endogenous theta oscillations can result in scores up to 0.3. (**g**) For 10-trial blocks with the longest sustained stimulation duration (i.e., with 10 s delay, average duration for stimulation sessions, 8 Hz: 392.6 s, 10 Hz: 392.5 s; 12 Hz: 410.0 s; 20 Hz: 345.4 s), pacing efficiency did not differ between the first and the second half of the block [n(8 Hz, 10 Hz, 12 Hz, 20 Hz) = 24, 28, 27, 16 mice, dots are individual data points, open circles and bars are median ± 25th to 75th percentile, $z = 0.37, -0.30, 0.82, 1.40$, $P = 0.71, 0.77, 0.41, 0.16$, two-sided Wilcoxon signed rank tests].

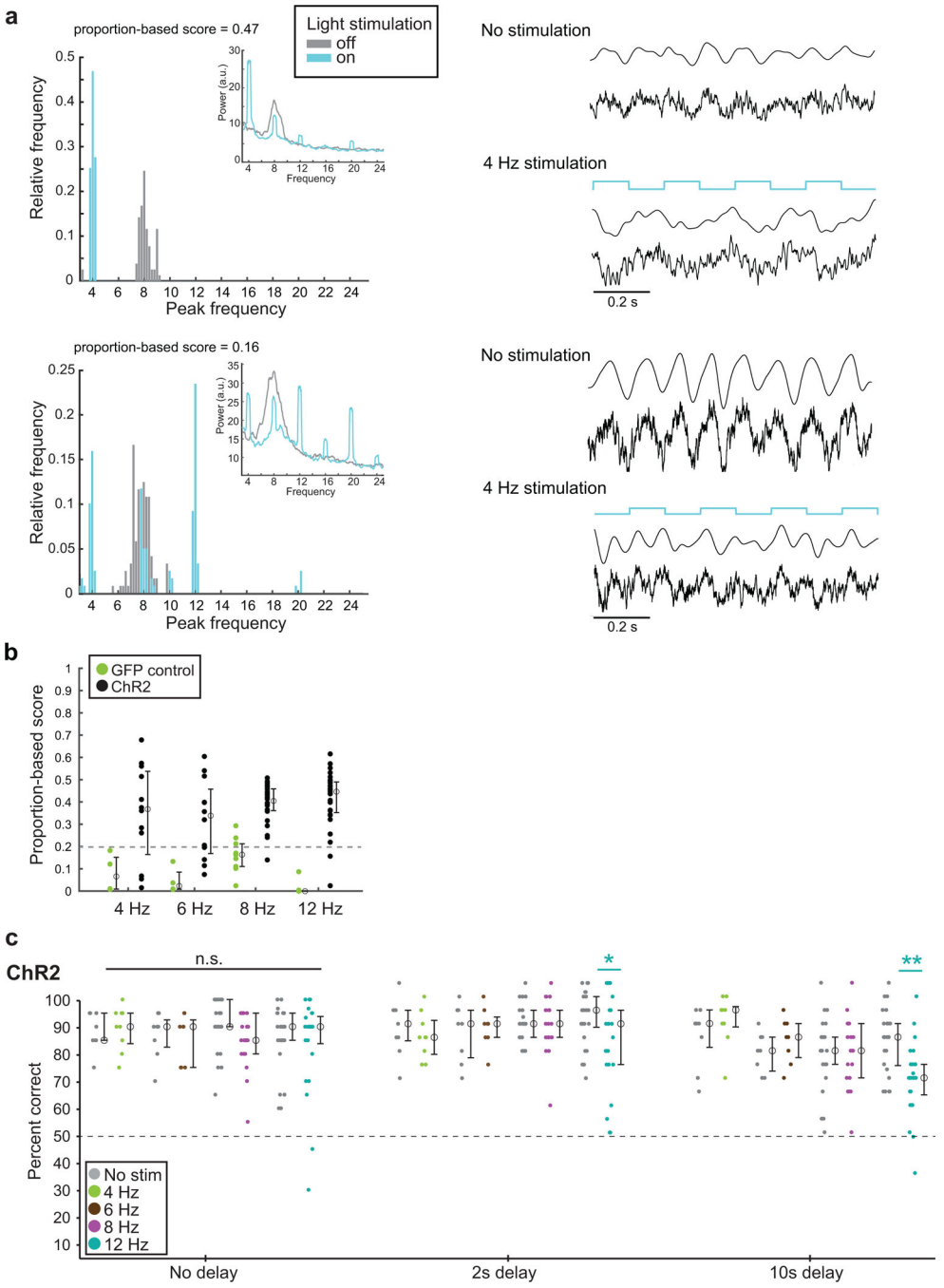

Extended Data Fig. 8. Pacing of oscillations at frequencies below 8 Hz did not result in memory impairment.

(**a**) Pacing was efficient with 4 Hz and 6 Hz stimulation in the majority of mice but harmonics were frequently observed. Distribution of the predominant frequency (*left*), power spectrum (*insert*), and example raw and filtered (3–22 Hz) waveforms (*right*) without stimulation and with 4 Hz stimulation in one mouse with weak harmonics (*top*) and one mouse with strong harmonics (*bottom*). (**b**) Proportion-based pacing scores at stimulation frequencies <8 Hz, and for comparison, at stimulation frequencies of 8 Hz and 12 Hz [*n*(4

Hz, 6 Hz, 8 Hz, 12 Hz) = 12, 12, 25, 29 mice]. Dots are individual data points, open circles and bars are median ± 25th to 75th percentile. When harmonics at 8 and 12 Hz were more pronounced the pacing efficiency score at 4 Hz was reduced [e.g., 0.16 in the bottom example in (a) is below the threshold of 0.2], such that these sessions were excluded from analysis of behavioral data (n = 3 at 4 Hz, 3 at 6 Hz). (**c**) Similar to the effect with 8 Hz stimulation, stimulation at 4 and 6 Hz did not result in impaired memory performance in the delayed spatial alternation task (No delay: n = 9 and 8, W = 14.0 and 6.5, P = 0.53 and 0.94; 2 s delay: W = 12.5 and 18.5, P = 0.48 and 0.59; 10 s delay: W = 25.0 and 20.5, P = 0.094 and 0.34, two-sided Wilcoxon signed rank tests). Dots are individual data points, open circles and bars are median ± 25th to 75th percentile. Data with 8 Hz and 12 Hz pacing are shown for comparison and correspond to the data shown in Fig. 8. * P < 0.05, ** P < 0.01, see Supplementary Table 3 for detailed statistics.

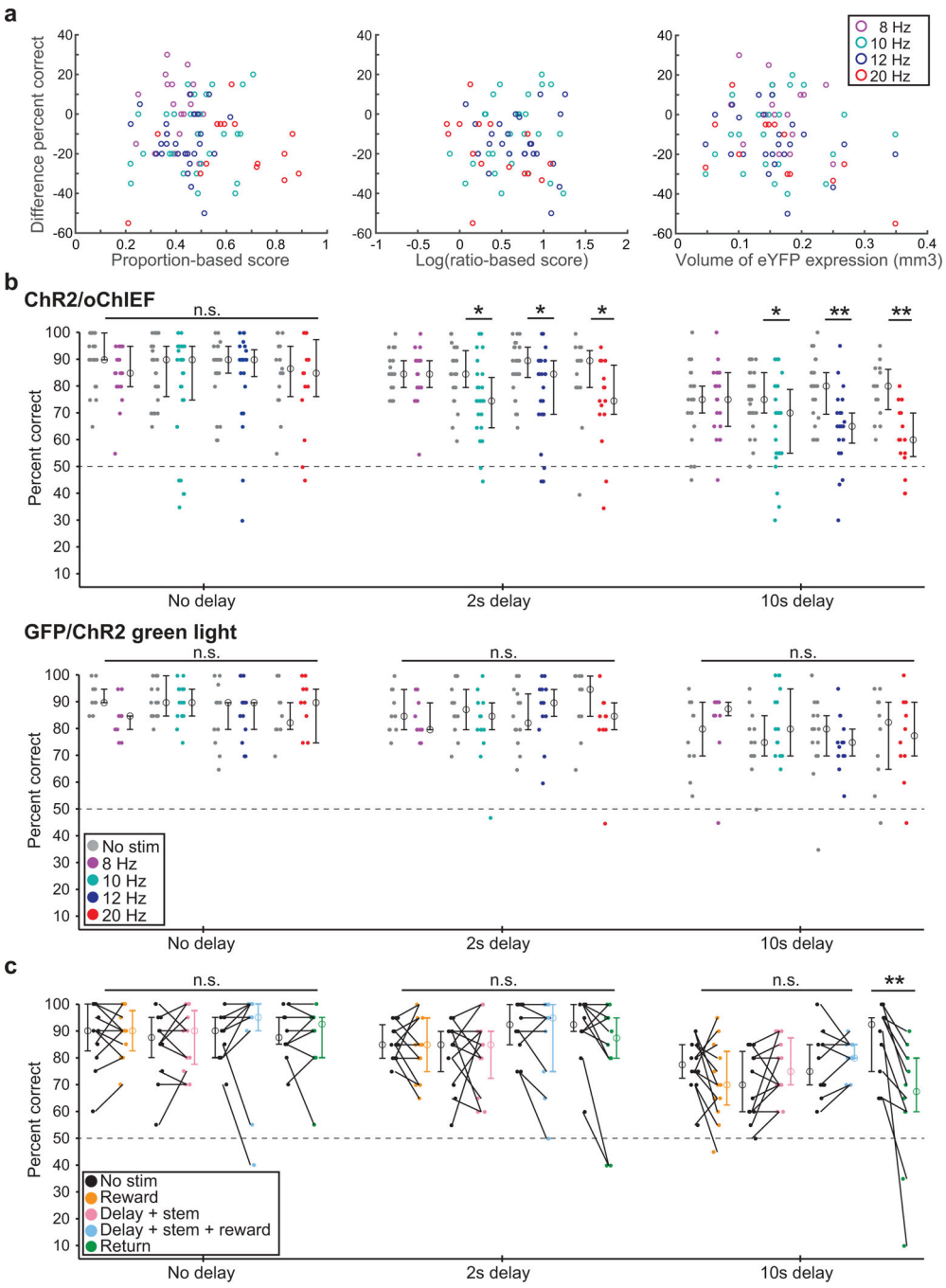

Extended Data Fig. 9. There was no relation between pacing efficiency and the decreased behavioral performance in the 10 s delay condition.

(**a**) Comparisons of the decrease in behavioral performance in the 10 s delay condition with either the pacing efficiency (*left*, proportion-based score; *middle*, ratio-based score) or the volume of viral vector expression in MSA (*right*) did not reveal any correlations at any stimulation frequency [ratio-based score, n(10, 12, 20 Hz) = 25, 24, 14; *rho* = 0.19, −0.086, −0.55; P = 0.35, 0.68, 0.033 (0.10, Holm-Bonferroni corrected); proportion-based score: n(8, 10, 12, 20 Hz) = 20, 25, 24, 14; *rho* = −0.12, 0.22, −0.01, −0.06; P = 0.60,

0.30, 0.96, 0.83; EYFP volume, *n*(8, 10, 12, 20 Hz) = 22, 26, 24, 14; *rho* = −0.16, 0.0096, −0.34, −0.59; *P* = 0.48, 0.96, 0.10, 0.027 (0.11, Holm-Bonferroni corrected), Spearman rank correlations]. (**b**) Behavioral data for no stimulation and stimulation sessions at each frequency. Dots are individual data points, open circles and bars are median ± 25th to 75th percentile. The experimental design included, for each of the three delay conditions on each day, blocks of 10 trials with stimulation and 10 trials without stimulation, and the difference in performance between stimulation and no-stimulation blocks was calculated to control for day-to-day variations in behavioral performance (as shown in Fig. 8c and e). Statistical analysis was thus performed on the difference in percent correct trials between blocks with and without stimulation [ChR2/oChIEF: *n*(8 Hz, 10 Hz, 12 Hz, 20 Hz) = 22, 27, 25, 15 mice, 2 s delay, *P* = 0.61, 0.021, 0.037, 0.037; 10 s delay, *P* = 0.86, 0.026, 0.0012, 0.0043, Holm-Bonferroni corrected, two-sided Wilcoxon signed rank tests; GFP/ChR2 green light: n = 10, 14, 14, 10 mice, all *P* values, n.s., two-sided Wilcoxon signed rank tests). See main text and Supplementary Table 3 for detailed statistics. (**c**) Behavioral data for sessions with stimulation that were targeted to maze zones [*n*(Reward, Delay+Stem, Delay+Stem+Reward, Return) = 12, 12, 10, 10 mice; 10 s delay/Return: *P* = 0.0078, Holm-Bonferroni corrected, two-sided Wilcoxon signed rank test; all other comparisons, n.s.]. Dots are individual data points, open circles and bars are median ± 25th to 75th percentile. Occupancy times in the stimulated zones were higher in the delay+stem+reward condition (medians: 8.96+1.94+6.78 s = 17.68 s) than in the return condition (median: 7.52 s) (Extended Data Fig. 10) such that time of stimulation cannot explain the selective effect of return-arm stimulation on behavioral performance. n.s., not significant, * $P < 0.05$, ** $P < 0.01$, two-sided Wilcoxon signed rank tests, see main text and Supplementary Table 3 for detailed statistics.

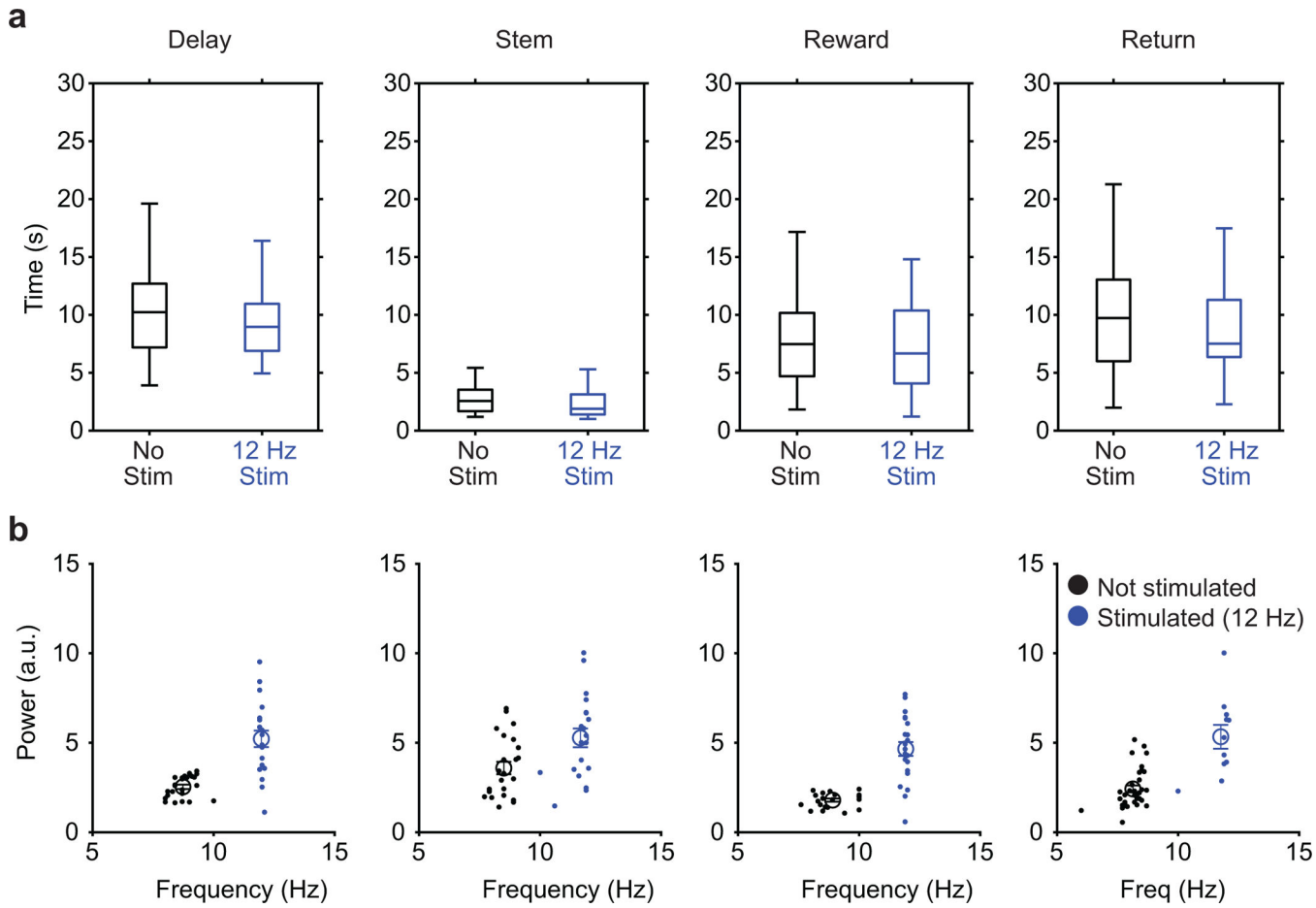

Extended Data Fig. 10. Length of light stimulation and magnitude of LFP power across maze segments did not explain the selective effect of return-arm stimulation on behavioral performance during 10 s delay trials.

(**a**) Time in each of the maze zones did not differ between no stimulation and stimulation trials [n(no stimulation, stimulation) = [39, 36], [39, 36], [36, 39], and [36, 39] sessions for Delay, Stem, Reward, and Return, z = 0.93, 1.12, 1.12, 0.53, P = 0.35, 0.26, 0.26, 0.59, two-sided Wilcoxon rank sum test]. Data are presented as boxplots (horizontal line in box: median, bottom and top of box: 25th and 75th percentiles, whiskers: most extreme values that are not outliers). Importantly, the median time in the return arms (7.52 s) was substantially lower than in the condition when stimulation was on during the delay+stem+reward (17.68 s), which indicates that the selective effect of return-arm stimulation on memory performance (Fig. 8e and Extended Data Fig. 9c) cannot be attributed to longer stimulation durations. (**b**) Baseline theta power differed between maze segments [H(3) = 22.76, $P = 4.5 \times 10^{-5}$, Kruskal-Wallis test; delay (n = 24 sessions) vs reward (n = 22 sessions): $P = 3.0 \times 10^{-4}$ (0.0015, Holm-Bonferroni corrected), stem (n = 24 sessions) vs reward (n = 24 sessions): $P = 3.4 \times 10^{-5}$ (0.00020, Holm-Bonferroni corrected), stem (n = 24 sessions) vs return (n = 33 sessions): P = 0.0053 (0.02, Holm-Bonferroni corrected); all other comparisons, n.s., two-sided Wilcoxon rank sum tests], but oscillation power corresponded across maze segments during 12 Hz pacing [n(Delay, Return, Reward, Stem) = 20, 11, 22, 20 sessions, H(3) = 0.77, P = 0.86, Kruskal-Wallis test]. Moreover,

oscillation frequency was reliably shifted to 12 Hz in each maze segment. Differences in pacing efficiency across maze segments therefore do not appear to contribute to the selective effect of return-arm stimulation on memory performance (Fig. 8e and Extended Data Fig. 9c). Dots are individual data points, open circles and bars are mean ± SEM.

Supplementary Material

Refer to Web version on PubMed Central for supplementary material.

ACKNOWLEDGEMENTS

We thank Matthew Robertson, Gecelle De Guia, and Sia Ahmadi for assistance, Byungkook Lim, Varoth Lilascharoen, and Eric Wang for providing viral vectors, Cory Root and Kiana Miyamoto for assistance with microscopy. This work was supported by NIH grant T32 GM007240 to C.R.Q, a Howard Hughes Medical Institute International Student Research Fellowship to I.Z, NIH grant R01 MH119179 and the Walter F. Heiligenberg Professorship to J.K.L, and NIH grants R01 NS102915, R21 MH100354, R01 NS084324, and R01 NS097772 to S. Leutgeb.

REFERENCES

1. Buzsaki G Theta rhythm of navigation: link between path integration and landmark navigation, episodic and semantic memory. Hippocampus 15, 827–840 (2005). [PubMed: 16149082]
2. Fries P A mechanism for cognitive dynamics: neuronal communication through neuronal coherence. Trends Cogn Sci 9, 474–480 (2005). [PubMed: 16150631]
3. Voytek B & Knight RT Dynamic network communication as a unifying neural basis for cognition, development, aging, and disease. Biol Psychiatry 77, 1089–1097 (2015). [PubMed: 26005114]
4. Ego-Stengel V & Wilson MA Disruption of ripple-associated hippocampal activity during rest impairs spatial learning in the rat. Hippocampus 20, 1–10 (2010). [PubMed: 19816984]
5. Jadhav SP, Kemere C, German PW & Frank LM Awake Hippocampal Sharp-Wave Ripples Support Spatial Memory. Science (2012).
6. Vosskuhl J, Struber D & Herrmann CS Non-invasive Brain Stimulation: A Paradigm Shift in Understanding Brain Oscillations. Front Hum Neurosci 12, 211 (2018). [PubMed: 29887799]
7. Petsche H, Stumpf C & Gogolak G [The significance of the rabbit's septum as a relay station between the midbrain and the hippocampus. I. The control of hippocampus arousal activity by the septum cells.]. Electroencephalogr Clin Neurophysiol 14, 202–211 (1962). [PubMed: 14038334]
8. Winson J Loss of hippocampal theta rhythm results in spatial memory deficit in the rat. Science 201, 160–163 (1978). [PubMed: 663646]
9. Hangya B, Borhegyi Z, Szilagyi N, Freund TF & Varga V GABAergic neurons of the medial septum lead the hippocampal network during theta activity. J Neurosci 29, 8094–8102 (2009). [PubMed: 19553449]
10. Freund TF & Antal M GABA-containing neurons in the septum control inhibitory interneurons in the hippocampus. Nature 336, 170–173 (1988). [PubMed: 3185735]
11. King C, Recce M & O'Keefe J The rhythmicity of cells of the medial septum/diagonal band of Broca in the awake freely moving rat: relationships with behaviour and hippocampal theta. Eur J Neurosci 10, 464–477 (1998). [PubMed: 9749709]
12. Brazhnik ES & Fox SE Action potentials and relations to the theta rhythm of medial septal neurons in vivo. Exp Brain Res 127, 244–258 (1999). [PubMed: 10452212]
13. Borhegyi Z, Varga V, Szilagyi N, Fabo D & Freund TF Phase segregation of medial septal GABAergic neurons during hippocampal theta activity. J Neurosci 24, 8470–8479 (2004). [PubMed: 15456820]
14. Simon AP, Poindessous-Jazat F, Dutar P, Epelbaum J & Bassant MH Firing properties of anatomically identified neurons in the medial septum of anesthetized and unanesthetized restrained rats. J Neurosci 26, 9038–9046 (2006). [PubMed: 16943562]

15. Varga V, et al. The presence of pacemaker HCN channels identifies theta rhythmic GABAergic neurons in the medial septum. J Physiol 586, 3893–3915 (2008). [PubMed: 18565991]
16. Joshi A, Salib M, Viney TJ, Dupret D & Somogyi P Behavior-Dependent Activity and Synaptic Organization of Septo-hippocampal GABAergic Neurons Selectively Targeting the Hippocampal CA3 Area. Neuron 96, 1342–1357 e1345 (2017). [PubMed: 29198757]
17. Bender F, et al. Theta oscillations regulate the speed of locomotion via a hippocampus to lateral septum pathway. Nature communications 6, 8521 (2015).
18. Dannenberg H, et al. Synergy of direct and indirect cholinergic septo-hippocampal pathways coordinates firing in hippocampal networks. J Neurosci 35, 8394–8410 (2015). [PubMed: 26041909]
19. Zutshi I, et al. Hippocampal Neural Circuits Respond to Optogenetic Pacing of Theta Frequencies by Generating Accelerated Oscillation Frequencies. Curr Biol 28, 1179–1188 e1173 (2018). [PubMed: 29628373]
20. Alonso A & Kohler C A study of the reciprocal connections between the septum and the entorhinal area using anterograde and retrograde axonal transport methods in the rat brain. J Comp Neurol 225, 327–343 (1984). [PubMed: 6725648]
21. Gonzalez-Sulser A, et al. GABAergic projections from the medial septum selectively inhibit interneurons in the medial entorhinal cortex. J Neurosci 34, 16739–16743 (2014). [PubMed: 25505326]
22. Mitchell SJ, Rawlins JN, Steward O & Olton DS Medial septal area lesions disrupt theta rhythm and cholinergic staining in medial entorhinal cortex and produce impaired radial arm maze behavior in rats. J Neurosci 2, 292–302 (1982). [PubMed: 7062110]
23. Mizumori SJ, Ward KE & Lavoie AM Medial septal modulation of entorhinal single unit activity in anesthetized and freely moving rats. Brain Res 570, 188–197 (1992). [PubMed: 1617411]
24. Jeffery KJ, Donnett JG & O'Keefe J Medial septal control of theta-correlated unit firing in the entorhinal cortex of awake rats. Neuroreport 6, 2166–2170 (1995). [PubMed: 8595195]
25. Brandon MP, et al. Reduction of theta rhythm dissociates grid cell spatial periodicity from directional tuning. Science 332, 595–599 (2011). [PubMed: 21527714]
26. Koenig J, Linder AN, Leutgeb JK & Leutgeb S The spatial periodicity of grid cells is not sustained during reduced theta oscillations. Science 332, 592–595 (2011). [PubMed: 21527713]
27. Buzsaki G, Leung LW & Vanderwolf CH Cellular bases of hippocampal EEG in the behaving rat. Brain Res 287, 139–171 (1983). [PubMed: 6357356]
28. Kamondi A, Acsady L, Wang XJ & Buzsaki G Theta oscillations in somata and dendrites of hippocampal pyramidal cells in vivo: activity-dependent phase-precession of action potentials. Hippocampus 8, 244–261 (1998). [PubMed: 9662139]
29. Yoder RM & Pang KC Involvement of GABAergic and cholinergic medial septal neurons in hippocampal theta rhythm. Hippocampus 15, 381–392 (2005). [PubMed: 15630696]
30. Chrobak JJ, Stackman RW & Walsh TJ Intraseptal administration of muscimol produces dose-dependent memory impairments in the rat. Behav Neural Biol 52, 357–369 (1989). [PubMed: 2556105]
31. Hasselmo ME What is the function of hippocampal theta rhythm?--Linking behavioral data to phasic properties of field potential and unit recording data. Hippocampus 15, 936–949 (2005). [PubMed: 16158423]
32. Benchenane K, et al. Coherent theta oscillations and reorganization of spike timing in the hippocampal- prefrontal network upon learning. Neuron 66, 921–936 (2010). [PubMed: 20620877]
33. Wang Y, Romani S, Lustig B, Leonardo A & Pastalkova E Theta sequences are essential for internally generated hippocampal firing fields. Nat Neurosci 18, 282–288 (2015). [PubMed: 25531571]
34. Kay K, et al. Constant Sub-second Cycling between Representations of Possible Futures in the Hippocampus. Cell 180, 552–567 e525 (2020). [PubMed: 32004462]
35. Witter MP, Groenewegen HJ, Lopes da Silva FH & Lohman AH Functional organization of the extrinsic and intrinsic circuitry of the parahippocampal region. Prog Neurobiol 33, 161–253 (1989). [PubMed: 2682783]

36. Einevoll GT, Kayser C, Logothetis NK & Panzeri S Modelling and analysis of local field potentials for studying the function of cortical circuits. Nat Rev Neurosci 14, 770–785 (2013). [PubMed: 24135696]
37. Kropff E, Carmichael JE, Moser MB & Moser EI Speed cells in the medial entorhinal cortex. Nature 523, 419–424 (2015). [PubMed: 26176924]
38. Ainge JA, van der Meer MA, Langston RF & Wood ER Exploring the role of context-dependent hippocampal activity in spatial alternation behavior. Hippocampus 17, 988–1002 (2007). [PubMed: 17554771]
39. Sabariego M, et al. Time Cells in the Hippocampus Are Neither Dependent on Medial Entorhinal Cortex Inputs nor Necessary for Spatial Working Memory. Neuron 102, 1235–1248 e1235 (2019). [PubMed: 31056352]
40. Zhang F, Wang LP, Boyden ES & Deisseroth K Channelrhodopsin-2 and optical control of excitable cells. Nat Methods 3, 785–792 (2006). [PubMed: 16990810]
41. Fuhrmann F, et al. Locomotion, Theta Oscillations, and the Speed-Correlated Firing of Hippocampal Neurons Are Controlled by a Medial Septal Glutamatergic Circuit. Neuron 86, 1253–1264 (2015). [PubMed: 25982367]
42. Yamamoto J, Suh J, Takeuchi D & Tonegawa S Successful execution of working memory linked to synchronized high-frequency gamma oscillations. Cell 157, 845–857 (2014). [PubMed: 24768692]
43. Ramirez S, et al. Creating a false memory in the hippocampus. Science 341, 387–391 (2013). [PubMed: 23888038]
44. Spellman T, et al. Hippocampal-prefrontal input supports spatial encoding in working memory. Nature 522, 309–314 (2015). [PubMed: 26053122]
45. Somogyi P, et al. Identified axo-axonic cells are immunoreactive for GABA in the hippocampus and visual cortex of the cat. Brain Res 332, 143–149 (1985). [PubMed: 3995258]
46. Salib M, et al. GABAergic Medial Septal Neurons with Low-Rhythmic Firing Innervating the Dentate Gyrus and Hippocampal Area CA3. J Neurosci 39, 4527–4549 (2019). [PubMed: 30926750]
47. Lepperod ME, et al. Optogenetic pacing of medial septum parvalbumin-positive cells disrupts temporal but not spatial firing in grid cells. Science advances 7 (2021).
48. Mizumori SJ, Barnes CA & McNaughton BL Reversible inactivation of the medial septum: selective effects on the spontaneous unit activity of different hippocampal cell types. Brain Res 500, 99–106 (1989). [PubMed: 2605512]
49. Pilly PK & Grossberg S How reduction of theta rhythm by medial septum inactivation may covary with disruption of entorhinal grid cell responses due to reduced cholinergic transmission. Front Neural Circuits 7, 173 (2013). [PubMed: 24198762]
50. Robbe D, et al. Cannabinoids reveal importance of spike timing coordination in hippocampal function. Nat Neurosci 9, 1526–1533 (2006). [PubMed: 17115043]
51. Robbe D & Buzsaki G Alteration of theta timescale dynamics of hippocampal place cells by a cannabinoid is associated with memory impairment. J Neurosci 29, 12597–12605 (2009). [PubMed: 19812334]
52. Lenck-Santini PP, Fenton AA & Muller RU Discharge properties of hippocampal neurons during performance of a jump avoidance task. J Neurosci 28, 6773–6786 (2008). [PubMed: 18596153]
53. Newman EL, et al. Precise spike timing dynamics of hippocampal place cell activity sensitive to cholinergic disruption. Hippocampus 27, 1069–1082 (2017). [PubMed: 28628945]
54. Kao HY, et al. Phencyclidine Discoordinates Hippocampal Network Activity But Not Place Fields. J Neurosci 37, 12031–12049 (2017). [PubMed: 29118102]
55. Lubenov EV & Siapas AG Hippocampal theta oscillations are travelling waves. Nature 459, 534–539 (2009). [PubMed: 19489117]
56. Hernandez-Perez JJ, Cooper KW & Newman EL Medial entorhinal cortex activates in a traveling wave in the rat. eLife 9 (2020).
57. Goutagny R, et al. Alterations in hippocampal network oscillations and theta-gamma coupling arise before Abeta overproduction in a mouse model of Alzheimer's disease. Eur J Neurosci 37, 1896–1902 (2013). [PubMed: 23773058]

58. Diehl GW, Hon OJ, Leutgeb S & Leutgeb JK Grid and Nongrid Cells in Medial Entorhinal Cortex Represent Spatial Location and Environmental Features with Complementary Coding Schemes. Neuron (2017).

59. Mitzdorf U Current source-density method and application in cat cerebral cortex: investigation of evoked potentials and EEG phenomena. Physiol Rev 65, 37–100 (1985). [PubMed: 3880898]

60. Makarov VA, Makarova J & Herreras O Disentanglement of local field potential sources by independent component analysis. J Comput Neurosci 29, 445–457 (2010). [PubMed: 20094907]

61. Belluscio MA, Mizuseki K, Schmidt R, Kempter R & Buzsaki G Cross-frequency phase-phase coupling between theta and gamma oscillations in the hippocampus. J Neurosci 32, 423–435 (2012). [PubMed: 22238079]

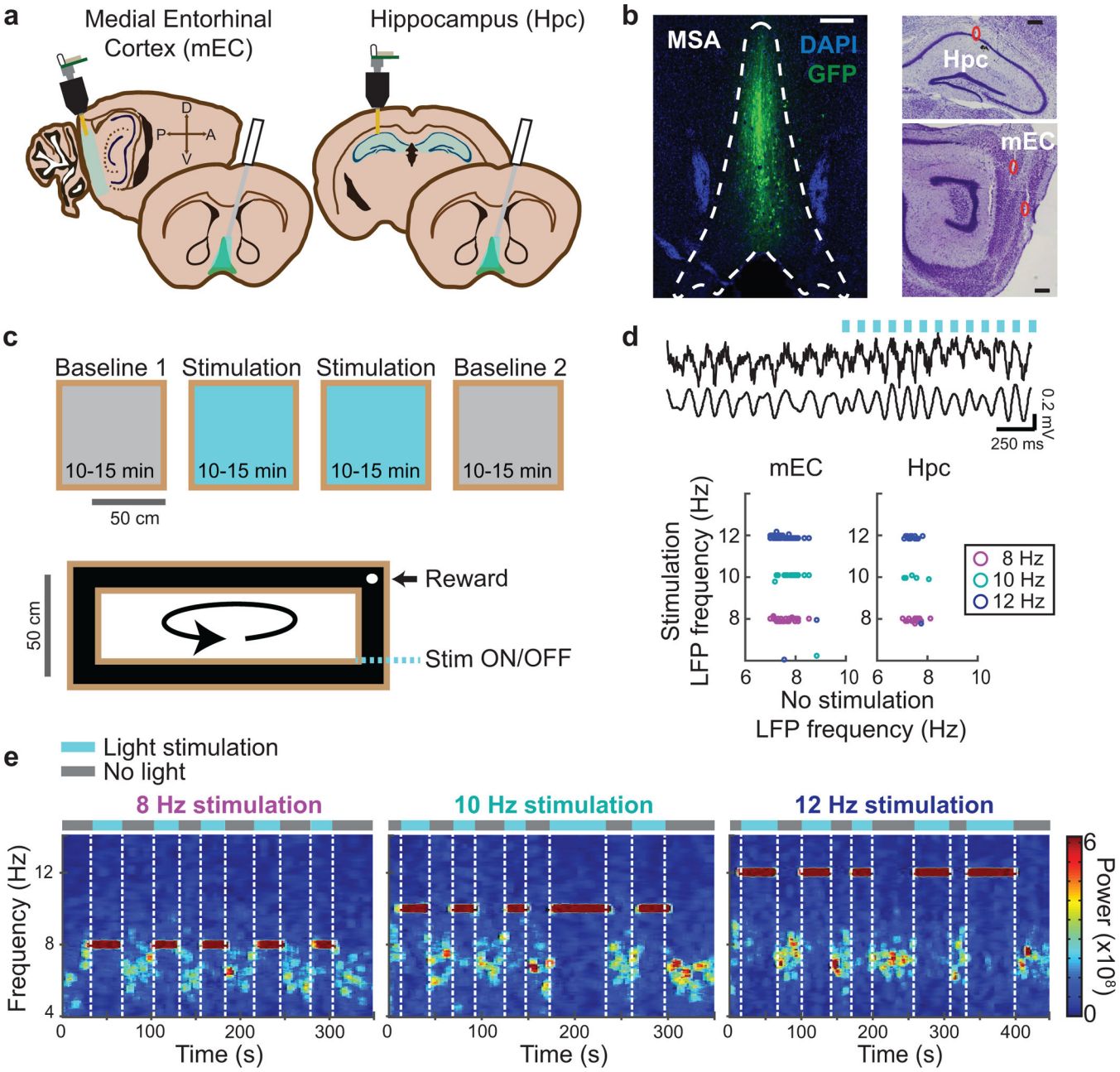

Figure 1. Rhythmic optogenetic stimulation of MSA PV neurons controlled the frequency of LFP oscillations in mEC and hippocampus of freely moving mice.

(**a**) Viral vectors were delivered to the MSA of PV-Cre mice to express either ChR2 or oCHIEF in PV cells. An optic fiber was placed just above the MSA and electrodes were lowered into either mEC (n = 11 mice) or hippocampus (Hpc, n = 4 mice). (**b**, *left*) Example image of the septal area shows GFP (green) that is coexpressed with opsin. Section is counterstained with DAPI (blue). (**b**, *right*) Example electrode tracks (red circles) in Hpc (*top*) and mEC (*bottom*). All scale bars are 250 μm. (**c**, *top*) Schematic of a recording sequence in the open field. (**c**, *bottom*) Schematic of the rectangular track. Arrow indicates running direction. Rhythmic stimulation was either turned on or off when the mouse crossed

a boundary (blue stippled line), such that laps with and without stimulation alternated. (**d**, *top*) Example mEC LFP recording before and during a train of blue light delivery shows the higher LFP frequency during periods with light stimulation. (**d**, *bottom*) During rhythmic optical stimulation of the MSA at 8, 10, or 12 Hz, mEC and Hpc peak LFP frequency reliably shifted from the endogenous theta frequency to closely match the stimulation frequency. Each dot is a recording session (mEC: n = 41, 22, and 59 sessions; Hpc: n = 20, 6, and 20 sessions for 8, 10 and 12 Hz stimulation, respectively). (**e**) Example mEC recordings from an individual mouse during rhythmic optical stimulation at 8, 10, and 12 Hz on every other lap of the track. During laps with stimulation, LFP oscillations immediately and persistently shifted to match the stimulation frequency, and the optogenetically paced oscillations superseded the endogenous theta (6–9 Hz) oscillation.

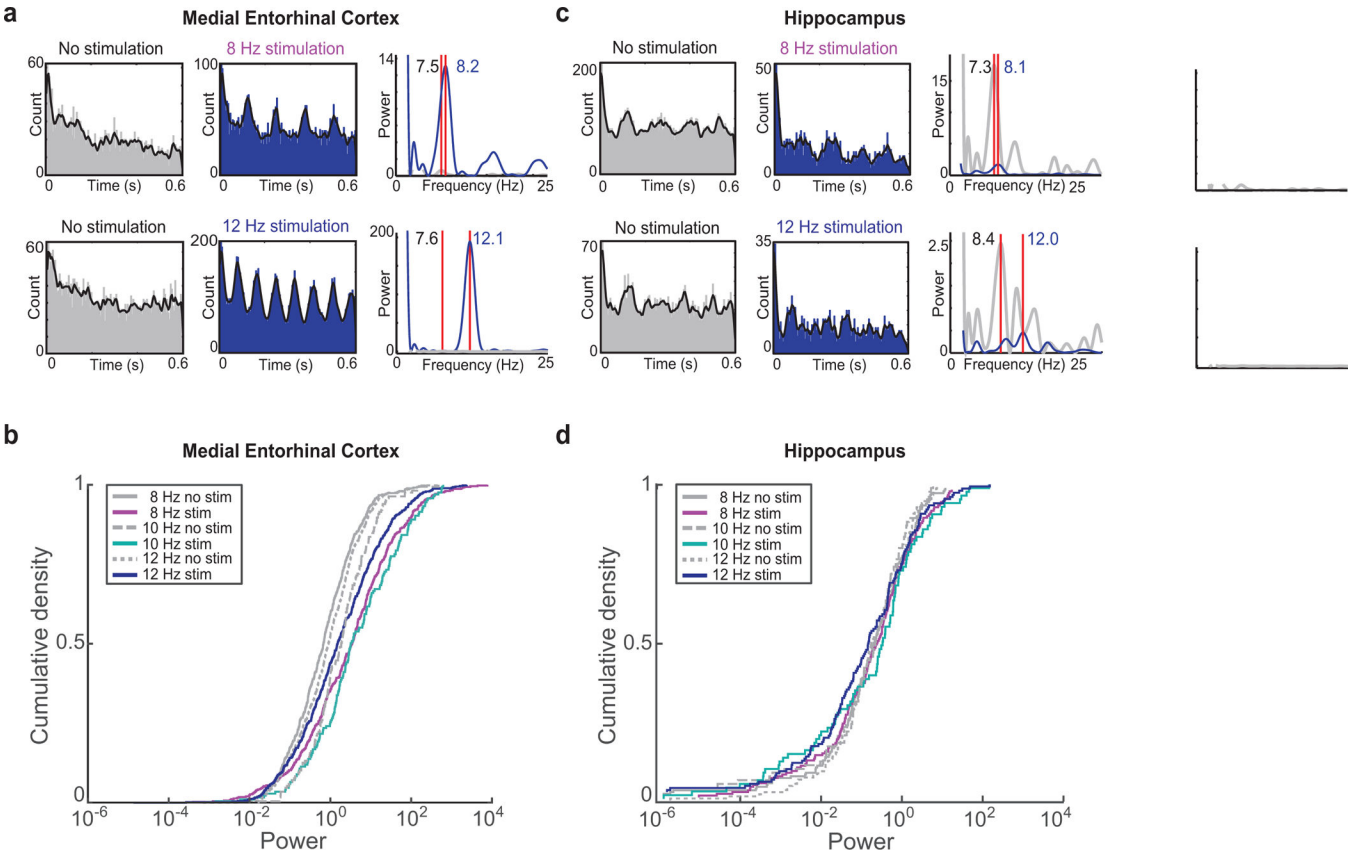

Figure 2. Pacing of MSA PV cells increased the oscillation amplitude of mEC cells, but not of hippocampal cells.

(**a**) Autocorrelation plots (*left*, *middle*) and FFT analysis (*right*) of the spike trains of two example mEC cells. Power and peak oscillation frequency in the 6–14 Hz range were calculated for each cell. (**b**) Cumulative density function of the power for all putative mEC principal cells during 8, 10, and 12 Hz stimulation (colored lines), and of the same cells during periods without stimulation (gray lines). (**c**, **d**) Same as in (a, b) but for putative CA1 principal cells. Septal stimulation increased the power of oscillations of mEC cells [n(8, 10, 12 Hz) = 479, 180, 591 cells in 11 mice, $K = 0.32, 0.23, 0.16$, $P = 1.1 \times 10^{-21}$, 0.00014, 1.9×10^{-7}, two-sided KS tests compared to no stimulation], but not of hippocampal cells [n(8, 10, 12 Hz) = 175, 80, 138 cells, $K = 0.06, 0.14, 0.14$, $P = 0.94, 0.34, 0.10$, two-sided KS tests compared to no stimulation]. The more pronounced effect on mEC compared to hippocampal cells was observed even though pacing scores at each frequency were either comparable to or lower than hippocampal pacing scores (mean pacing score with 8, 10 and 12 Hz stimulation: mEC: 0.27, 0.40, 0.34; hippocampus: 0.38, 0.43, and 0.33).

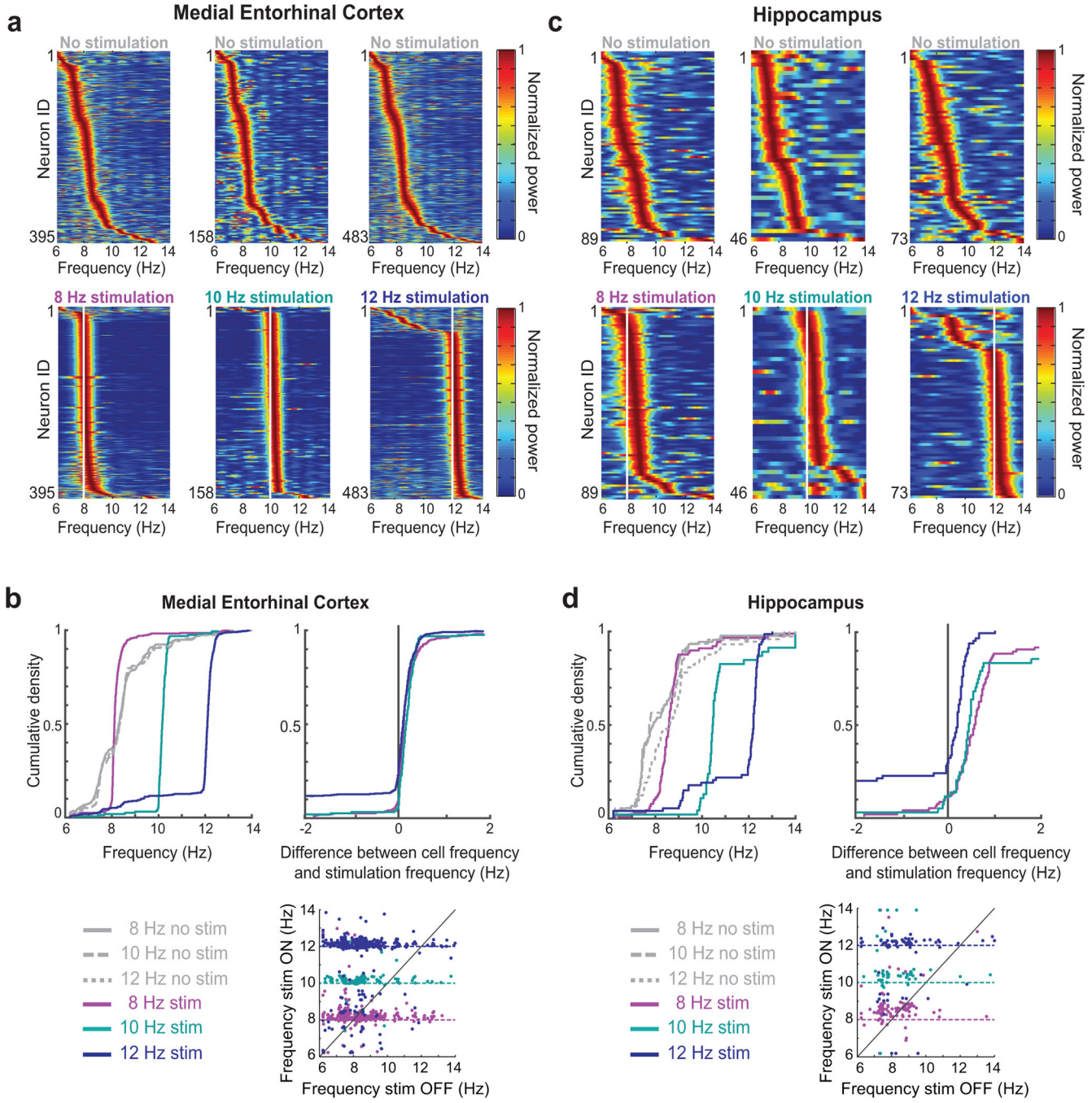

Figure 3. Firing of mEC cells was entrained to oscillation frequencies that closely corresponded to pacing frequencies.

(**a**) Oscillatory firing of the spike trains of all putative principal cells in mEC. Each line in color-coded panels is the normalized power of the oscillations of spike trains at frequencies between 6 and 14 Hz. Within each panel, cells are ordered by their peak oscillation frequency. Cells with power <0.1 were excluded because frequency could not be accurately estimated. Vertical white lines indicate stimulation frequency. (**b**, *left*) Cumulative density function of the entrainment of the cells' spike trains to 8, 10, and 12 Hz pacing frequencies

(colored lines), and of the same cells' spike train oscillations during periods without stimulation (gray lines). (**b**, *bottom*) The spiking of most mEC cells became entrained to the stimulation frequency, irrespective of their preferred spiking frequency at baseline. (**b**, *right*) Cumulative density function of the difference between the spike train's oscillation frequency and the stimulation frequency. For 8, 10, and 12 Hz stimulation (n = 395, 158, 483 cells), the median difference (±iqr) to the stimulation frequency is 0.11 Hz(±0.18), 0.16 Hz(±0.20), and 0.10 Hz(±0.21), respectively. (**c**, **d**) Same as in (a, b) but for hippocampal principal cells. Hippocampal cells showed differences from the stimulation frequency [n(8, 10, 12 Hz) = 89, 46, 71 cells, median difference (±iqr) = 0.59 (±0.54), 0.46 (±0.34), 0.21 (±0.35)], which were larger than for mEC (Z = −8.92, −6.17, −2.10, $P = 4.6 \times 10^{-19}$, 6.9×10^{-10}, 0.035, two-sided Wilcoxon rank sum tests).

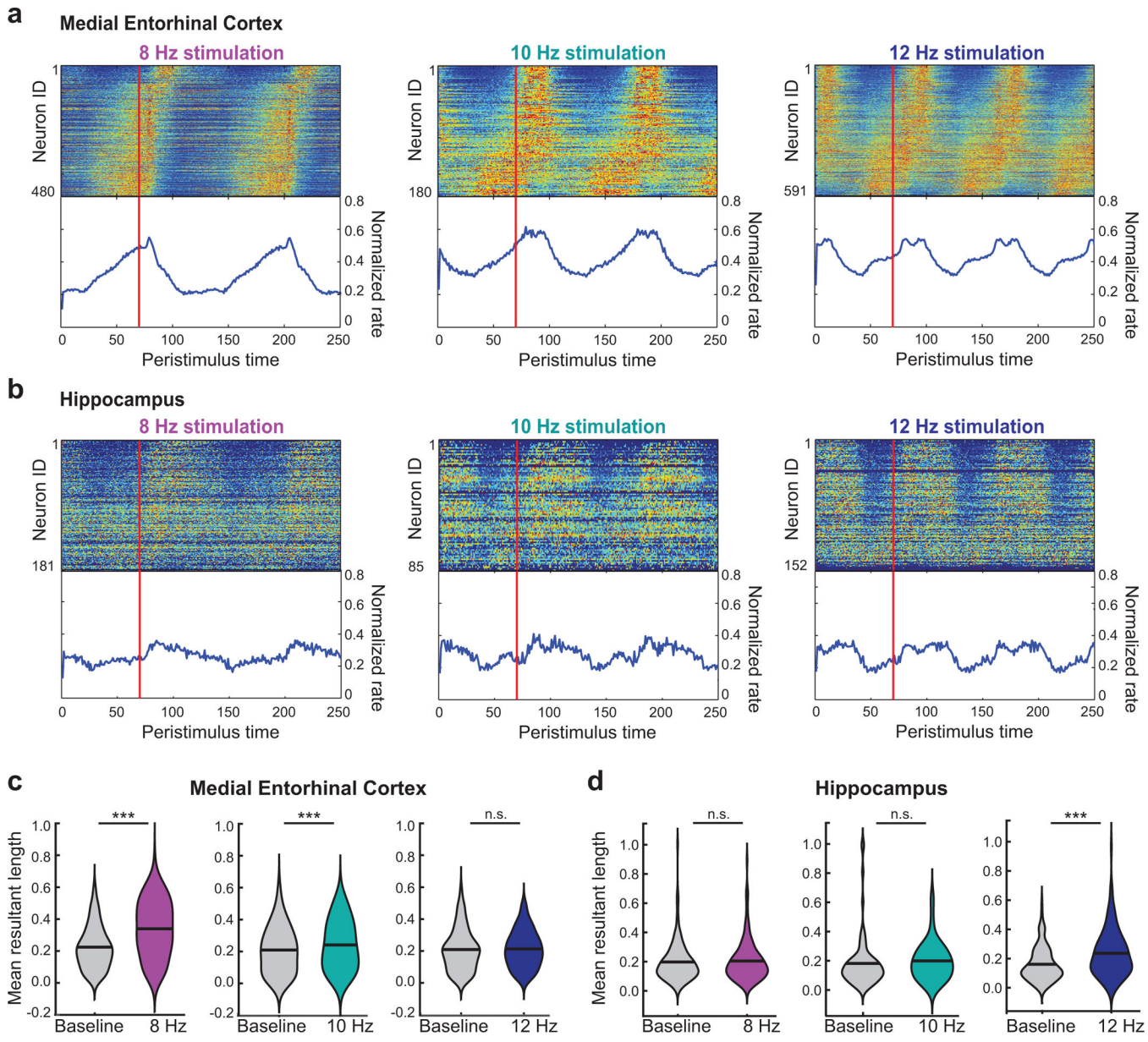

Figure 4. Medial entorhinal cells were more strongly entrained to septal stimulation than hippocampal cells.

(**a**) Peri-stimulus time histograms show the normalized rate of each mEC cell (*top*, color coded with the same color scheme as in Fig. 3) and the average over all normalized rates (*bottom*). Red vertical line is the light onset, and 250 ms are plotted to show approximately two cycles. (**b**) Same as (a), but for hippocampus. The relative increase in firing rate in the 30 ms following the onset of the optical stimulation was higher in mEC principal cells than in hippocampal CA1 principal neurons [mEC: n(8, 10, 12 Hz)= 480, 180, 591 cells; median (±iqr) = 1.62 (±1.90), 1.59 (±1.54), 1.42 (±0.92); hippocampus: n(8, 10, 12 Hz) = 181, 85, 152 cells; median (±iqr) = 1.46 (±1.03), 1.29 (±0.61), 1.23 (±0.78); mEC vs. hippocampus: z = 2.08, 3.26, 3.22, P = 0.037, 0.0011, 0.0013, two-sided Wilcoxon rank sum tests) (**c**) Phase locking between spiking and LFP oscillations in the 6–14 Hz range

is obtained by first determining the phase of each spike and by then calculating the mean resultant length from all spike phases during periods with and without stimulation. Violin plots show the distribution of all cells' resultant lengths for each stimulation condition [n(8, 10, 12 Hz) = 436, 193, 639 cells, baseline vs. stimulation: z = −15.92, −5.55, −1.07, P = 4.8 × 10^{-55}, 1.4 × e^{-5}, 0.29, two-sided Wilcoxon paired signed-rank tests]. (**d**) Same as (c), but for hippocampus [n(8, 10, 12 Hz) = 181, 84, 152 cells, baseline vs. stimulation: z = −0.31, −1.71, −6.07, P = 0.76, = 0.088, 1.3 × 10^{-9}, two-sided Wilcoxon paired signed-rank tests]. *** P < 0.001, n.s., not significant.

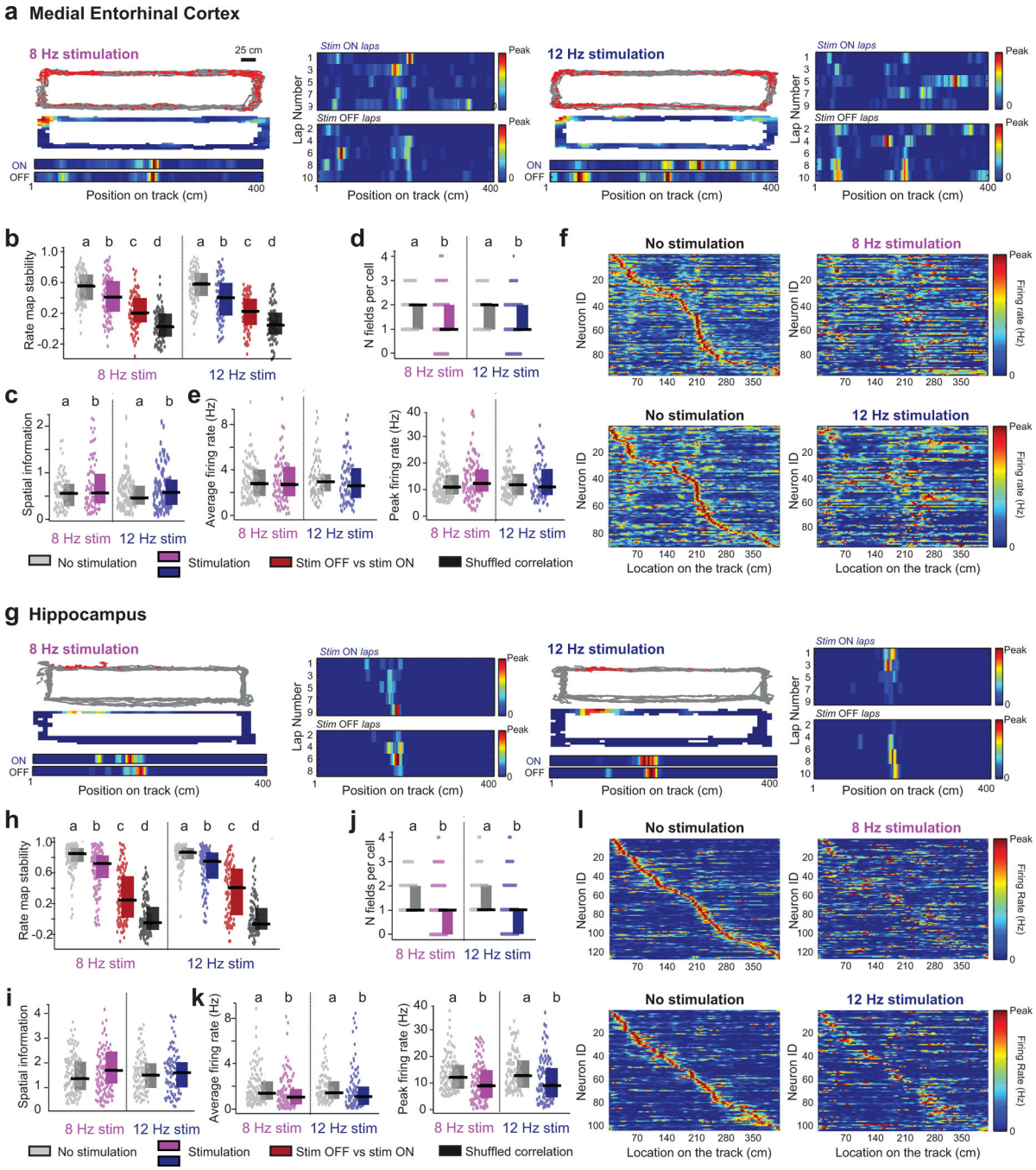

Figure 5. Effects on spatial firing patterns were corresponding across stimulation frequencies.

(**a**) Example spatial firing patterns of mEC cells recorded during sessions with 8 Hz (*left*) and 12 Hz pacing (*right*). The entire session is shown by plotting spike position (red dots) on the trajectory and the firing rates relative to the peak rate as a heat map. Firing rates are also shown in a linearized heat map, and individual trials with and without stimulation are plotted as heat maps. Spatial firing was observed during trials with and without optical stimulation. (**b**) Spatial correlations across laps differed between all 4 types of comparisons [within light-off, within light-on, between light-off/on, with cell identify shuffled, 8 Hz and

12 Hz: n = 98 and 86 cells in 2 mice, $\chi^2(3)$ = 129.3 and 121.4, $P = 7.3 \times 10^{-30}$ and 6.5×10^{-28}, Friedman tests followed by two-sided Dunn Bonferroni rank sum difference, P values for all pairwise differences < 0.01]. Individual data points are shown as dots, the median as a horizontal line, and the 25th to 75th percentile interval as a box. Different letters above columns indicate significant differences. The pattern of results indicates that remapping was partial (i.e., between light-off/on value is higher than for shuffle but lower than within light off and within light on values). Similar remapping also occurs in response to light stimulation in GFP control mice (Extended Data Fig. 5). In addition, the higher values for within light-off stability and within light-on stability indicates stable spatial organization within each condition. (**c**) Spatial information even showed an increase during light-on compared to light-off (8 and 12 Hz: n = 98 and 86 cells, $z = -3.57$ and -2.38, $P = 0.00022$ and 0.017, two-sided Wilcoxon signed rank tests). (**d**) The number of fields per cell decreased (8 and 12 Hz: n = 98 and 86 cells, $z = 1.96$ and 4.34, $P = 0.049$ and 0.00025, two-sided Wilcoxon signed-rank tests) consistent with a sharpening of the spatial firing patterns. (**e**) Mean and peak firing rate were not altered by light stimulation (average and peak rate, 8 Hz: n = 98 cells, $z = -0.25$ and -1.36, $P = 0.80$ and 0.17; 12 Hz: n = 86 cells, $z = 0.81$ and -0.79, $P = 0.42$ and 0.43, two-sided Wilcoxon signed-rank tests). (**f**) Positions of the spatial fields of mEC principal cells on the rectangular track are linearized and ordered left to right according to the position during light-off sessions. The reorganization across no stimulation and stimulation laps reflects remapping. (**g-l**) Same as (a-f) but for hippocampal principal cells. (**h**) Spatial correlations differed between all 4 comparisons [within light-off, within light on, between light-off/on, with cell identify shuffled, 8 and 12 Hz: n = 127 and 104 cells in 4 mice, $\chi 2(3)$ = 245.3 and 207.8, $P = 1.4 \times 10^{-54}$ and 8.5×10^{-47}; Friedman tests followed by Dunn Bonferroni rank sum difference, P values for all pairwise differences <0.05]. Similar remapping was previously shown to be a consequence of light stimulation alone in GFP control mice and is thus unrelated to the pacing of oscillations[19]. (**i-k**) Spatial information did not differ between light-off and light-on, while other firing properties showed a decrease during light-off compared to light-on, but to a similar extent for the 8 Hz and 12 Hz stimulation (spatial information, number of fields per cell, mean firing rate, peak firing rate, 8 Hz: n = 127 cells, $z = -0.23$, 4.99, 4.01, 4.62, $P = 0.82$, 6.1×10^{-7}, 6.1×10^{-5}, 3.9×10^{-6}; 12 Hz: n = 104 cells; $z = -0.54$, 4.29, 2.46, 3.97, $P = 0.59$, 1.8×10^{-5}, 0.014, 7.2×10^{-5}, two-sided Wilcoxon signed-rank tests). The matching effects on spatial firing for 8 Hz compared to 12 Hz stimulation were also confirmed with a two-way ANOVA (see Supplementary Table 1 for detailed statistics). Individual data points are shown as dots, the median as a horizontal line, and the 25th to 75th percentile interval as a box.

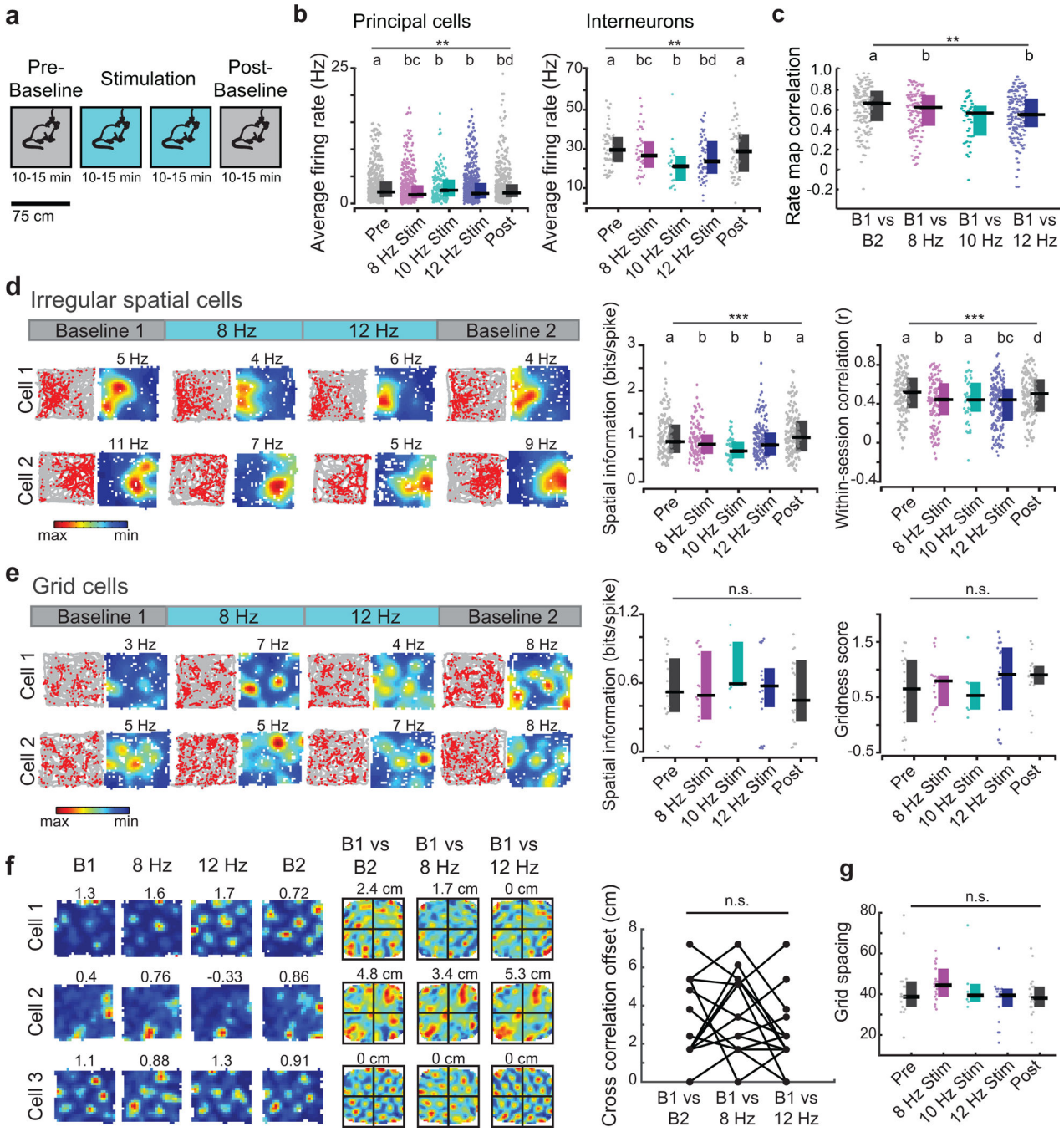

Figure 6. Spatial firing patterns in mEC matched across pacing frequencies, and grid coding was not altered by pacing in the open field.

(**a**) mEC cells were recorded while mice (n = 11) performed a random foraging task for 3–5 sessions per day. No stimulation was delivered during the first and last session, and continuous rhythmic stimulation at either 8, 10, or 12 Hz was delivered during each of the intervening stimulation sessions. (**b**) The average firing rate of mEC principal cells [*n*(B1, 8 Hz, 10 Hz, 12 Hz, B2) = 593, 477, 170, 589, 592 in 11 mice] and interneurons [*n*(B1, 8 Hz, 10 Hz, 12 Hz, B2) = 25, 17, 17, 14, 25 in 11 mice] showed minor differences

between conditions with and without light stimulation ($H(4, 2416) = 16.24$, $P = 0.0027$; interneurons: $n = 58, 42, 23$, and 55; mean rate: $H(4,231) = 14.05$, $P = 0.0071$, Kruskal-Wallis tests), but for principal cells at the 10 Hz and 12 Hz stimulation only compared to the pre-stimulation and not the post-stimulation baseline. Columns marked with *a* differ from *b*, and those marked with *c* differ from *d* (two-sided Wilcoxon rank-sum tests, Holm-Bonferroni corrected). See Extended Data Fig. 6 for peak rate. (**c**) Cells were classified as irregular spatial cells when their spatial information exceeded the 95th percentile of values from shuffled patterns in at least two recording sessions. Rate map correlations between the pre-stimulation baseline and session with either 8 Hz or 12 Hz pacing showed a decrease compared to rate map correlations between the pre-stimulation and the post-stimulation baseline [n(B1 vs B2, B1 vs 8 Hz, B1 vs 10 Hz, B1 vs 12 Hz) = 152, 125, 44, 152 spatial cells from 11 mice, $H(4,231) = 14.05$, $P = 0.0071$, Kruskal-Wallis test]. (**d**, *left*) Two example irregular spatial cells (spatial non-grid cells) are shown. Firing patterns in each of the four recording sessions are depicted by plotting spike locations (red dots) on top of the trajectory (gray lines) and by plotting the average firing rates at each location as a heat map. (**d**, *right*) Spatial information of irregular spatial cells showed a small decrease between sessions with and without light stimulation, but did not differ between any of the light stimulation frequencies [n(B1, 8 Hz, 10 Hz, 12 Hz, B2) = 152, 125, 44, 152, 152 spatial cells from 11 mice, $H(4,620) = 27.84$, $P = 1.35 \times 10^{-5}$, Kruskal-Wallis test]. The consistency of spatial firing patterns (within-session correlation) of irregular spatial cells was decreased at the 8 Hz and 12 Hz frequency compared to the pre-stimulation baseline but only at the 12 Hz frequency compared to the post-stimulation baseline ($H(4,620) = 20.07$, $P = 0.00048$, Kruskal-Wallis test). (**e**, *left*) Two example grid cells are plotted as in (d). (**e**, *right*) Grid cells were identified by gridness scores above the 95th percentile of scores from shuffled data in at least two recording sessions. Values below criterion can thus be observed in a subset of sessions, including baseline sessions with no light stimulation. The precision (spatial information) and regularity (gridness score) of grid cells did not differ between any of the stimulation conditions [n(B1, 8 Hz, 10 Hz, 12 Hz, B2) = 18, 18, 6, 18, 18 grid cells in 11 mice, spatial information: $H(4,73) = 2.151$, $P = 0.71$; gridness score: $H(4,73) = 2.42$, $P = 0.66$, Kruskal-Wallis tests]. (**f**) Panels to the left are the firing maps of grid cells in a series of 4 recording sessions (B1, 8 Hz, 12 Hz, B2; color scale is from zero in blue to maximum rate in red, grid scores are indicated on top). Panels to the right are the spatial crosscorrelation between sessions (B1 vs B2, B1 vs 8 Hz, B1 vs 12 Hz, color scale is from minimum in blue to maximum in red, offset of the central peak from the origin is indicated on top). Grid patterns did not shift during light stimulation sessions compared to sessions without stimulation, as measured by the offset of the central peak from the origin in the spatial crosscorrelograms ($n = 18$ grid cells, $\chi^2(2) = 0.90$, $P = 0.64$, Friedman test; Friedman test). (**g**) Grid spacing was not altered by light stimulation [n(B1, 8 Hz, 10 Hz, 12 Hz, B2) = 18, 18, 6, 18, 18 grid cells in 11 mice, $H(4,73) = 5.62$, $P = 0.23$, Kruskal-Wallis test). Individual data points are shown as dots, the median as a horizontal line, and the 25th to 75th percentile interval as a box. ** $P < 0.01$, *** $P < 0.001$. See Supplementary Table 2 for detailed statistics.

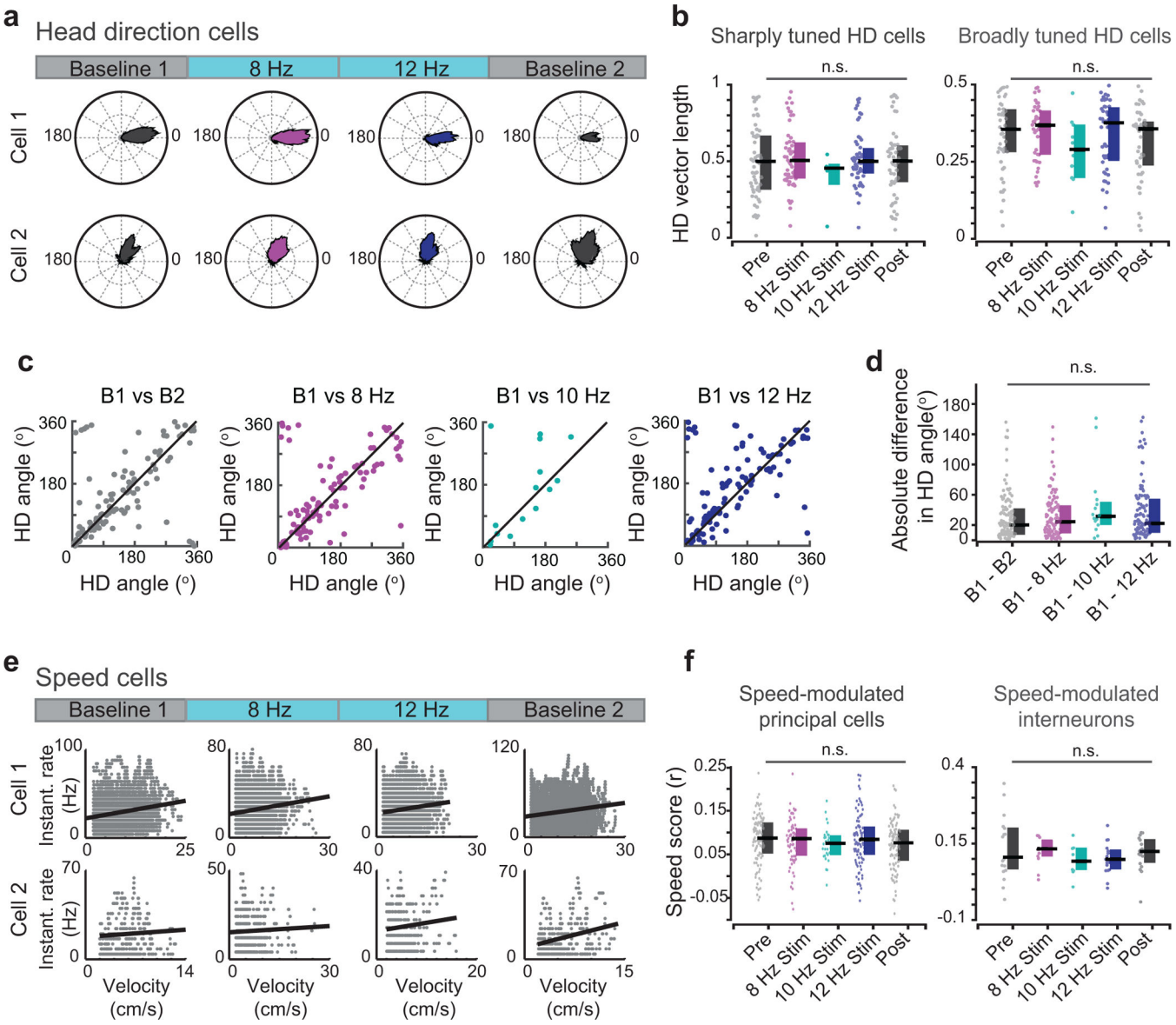

Figure 7. Head direction and speed coding were not disrupted when pacing oscillations at frequencies between 8–12 Hz.

(**a**) The directional tuning of two example head direction cells is shown in circular plots of firing rates by head direction. (**b**) The sharpness (i.e., HD vector length) of either sharply or broadly tuned HD cells did not differ across stimulus conditions [*n*(B1, 8 Hz, 10 Hz, 12 Hz, B2) = 58, 55, 5, 58, 58 sharply tuned HD cells in 11 mice, $H(4, 229) = 1.41$, $P = 0.84$; *n*(B1, 8 Hz, 10 Hz, 12 Hz, B2) = 47, 42, 10, 47, 47 broadly tuned HD cells in 11 mice, $H(4,188) = 4.51$, $P = 0.34$, Kruskal-Wallis tests]. (**c** and **d**) The head direction angle during the pre-stimulation baseline (B1) is compared to the angle in post-stimulation baseline (B2), 8 Hz, 10 Hz and 12 Hz stimulation sessions. The tuning angle of HD cells was not altered by MSA stimulation [*n*(B1, 8 Hz, 10 Hz, 12 Hz) = 105, 97, 15, 105 cells in 11 mice, $H(3, 318) = 2.98$, $P = 0.40$, Kruskal-Wallis test]. (**e**) Speed is plotted against instantaneous firing rate (Instant. rate), and regression lines are shown in black. (**f**) Average speed scores (r

values of the regression lines) of neither speed-modulated principal cells [n(B1, 8 Hz, 10 Hz, 12 Hz, B2) = 97, 72, 31, 97, 96, $H(4, 388) = 5.38$, $P = 0.25$, Kruskal-Wallis test] nor of speed-modulated interneurons [n(B1, 8 Hz, 10 Hz, 12 Hz, B2) = 18, 11, 8, 17, 18, $H(4, 67) = 2.81$, $P = 0.59$, Kruskal-Wallis test] differed between any of the stimulation conditions. Individual data points are shown as dots, the median as a horizontal line, and the 25th to 75th percentile interval as a box. n.s., not significant, see Supplementary Table 2 for detailed statistics.

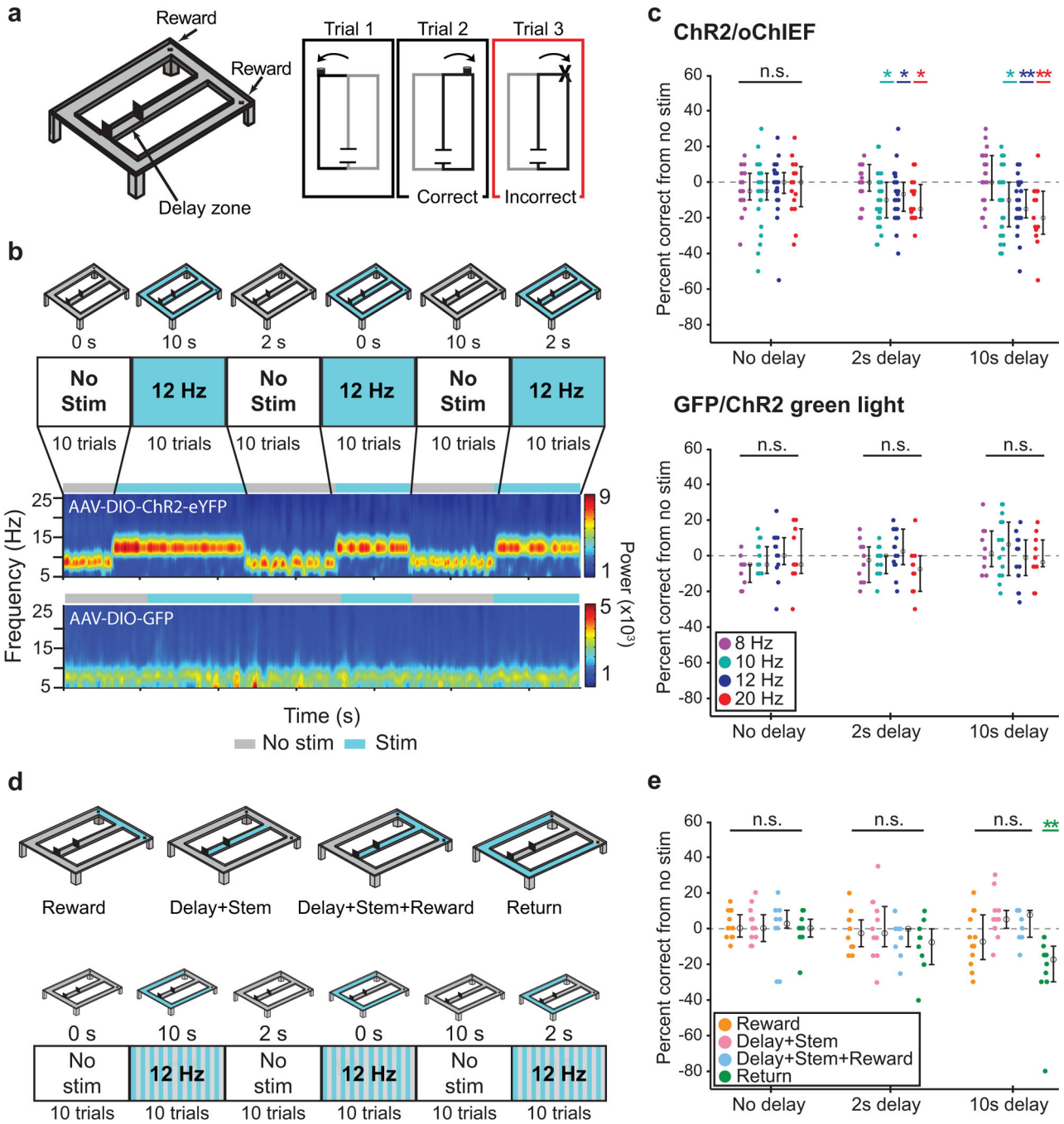

Figure 8. Spatial memory deficits emerged at pacing frequencies of 10, 12, and 20 Hz.

(**a**) Mice that expressed either opsins (ChR2 or oCHIEF) or GFP were trained in a spatial alternation task with no delay, 2 s delay and 10 s delay. (**b**) Once mice performed the task with high accuracy, they were tested in alternating blocks with and without light stimulation of the MSA. One stimulation frequency per day was selected, and different stimulation frequencies (i.e., 8, 10, 12, and 20 Hz) were used across days. An example session with 12 Hz stimulation is shown, along with a time-frequency spectrogram of the LFP. During stimulation periods, LFP oscillation frequency consistently matched the stimulation

frequency and replaced endogenous theta oscillations. For comparison, an example 12 Hz session in a GFP-expressing control mouse is shown, where blue light stimulation did not alter ongoing LFP. (**c**, *top*) In mice with opsin expression, blue light stimulation did not have any effect on behavior at the 8 Hz frequency ($n = 22$, no delay: $W = 47.5$, $P = 0.09$; 2 s delay: $W = 74.0$, $P = 0.61$; 10 s delay: $W = 89.5$, $P = 0.86$, two-sided Wilcoxon paired signed-rank tests), but impaired performance in trials with 2 s and 10 s delays for stimulation at 10, 12, or 20 Hz ($n = 27$, 25, and 15, no delay: $W = 98.5$, 94.0, 36.0, $P = 0.14$, 0.97 and 0.54; 2 s delay: $W = 42.5$, 41.0, 9.0, $P = 0.021$, 0.037 and 0.037, Holm-Bonferroni corrected; 10 s delay: $W = 43.0$, 16.0, 7.0, $P = 0.026$, 0.0012, and 0.0043, Holm Bonferroni corrected, two-sided Wilcoxon paired signed-rank tests). (**c**, *bottom*) There was no effect of stimulation in mice with GFP expression and in ChR2 mice with green light stimulation [n(8, 10, 12, 20 Hz) = 10, 14, 14, 10; no delay: $W = 3$, 37, 31, 29, $P = 0.092$ (Holm-Bonferroni corrected), 0.60, 0.77, 0.92; 2-s delay: $W = 15.5$, 11.5, 50.0, 6, $P = 0.46$, 0.25, 0.42, 0.10; 10 s delay: $W = 26.5$, 64.5, 46.0, 21.5, $P = 0.28$, 0.20, 0.70, 0.99, two-sided Wilcoxon paired signed-rank tests). (**d**) Optogenetic stimulation at 12 Hz was restricted to various zones of the maze, including (1) arm segments with reward, (2) stem+delay zone, (3) delay+stem+reward segments, and (4) return arms. One zone per day was selected, and different zones were tested across days. (**e**) There was no effect on memory performance during stimulation in zones 1–3 ($n = 12$, 12, 10; no delay: $W = 24.5$, 30.5, 15.0, $P = 0.91$, 0.82, 0.94; 2 s delay: $W = 19.5$, 33.5, 2.5, $P = 0.45$, 1, 0.25; 10 s delay: $W = 22.5$, 44.0, 32.0, $P = 0.21$, 0.090, 0.25). Stimulation on the return arms resulted in a decreased performance during 10 s delay trials ($n = 10$, $W = 0$, $P = 0.0078$, Holm-Bonferroni corrected, two-sided Wilcoxon paired signed-rank test) and a trend towards a decrease during 2-s delay trials ($n = 10$, $W = 6.5$, $P = 0.067$, two-sided Wilcoxon paired signed-rank tests). No effect was found without delay ($W = 11$, $P = 0.94$, two-sided Wilcoxon signed rank tests). Individual data points are shown as dots, the median as an open circle, and the 25^{th} to 75^{th} percentile interval as error bars. * $P < 0.05$, ** $P < 0.01$, n.s., not significant, see Supplementary Table 3 for detailed statistics.